Article

Increasing Reservoir Recovery Efficiency through Laboratory-Proven Hybrid Smart Water-Assisted Foam (SWAF) Flooding in Carbonate Reservoirs

Anas M. Hassan [1,*], Mohammed Ayoub [2], Mysara Eissa [2], Emad W. Al-Shalabi [1], Abdullah Al-Mansour [3] and Abdulrahman Al-Quraishi [3]

[1] Petroleum Engineering Department, Khalifa University of Science and Technology, Abu Dhabi P.O. Box 127788, United Arab Emirates; emad.walshalabi@ku.ac.ae

[2] Petroleum Engineering Department, Universiti Teknologi PETRONAS (UTP), Perak 32610, Malaysia; abdalla.ayoub@utp.edu.my (M.A.); mysara.eissa@utp.edu.my (M.E.)

[3] King Abdulaziz City for Science and Technology (KACST), Al Raed, Riyadh 12354, Saudi Arabia; aalmansour@kacst.edu.sa (A.A.-M.); aqurishi@kacst.edu.sa (A.A.-Q.)

* Correspondence: anas.hassan@ku.ac.ae

Abstract: This contribution introduces a new hybrid enhanced oil recovery (EOR) method which combines smart water-assisted foam (SWAF) flooding, known as the SWAF process. The concept of applying SWAF flooding in carbonate reservoirs is a novel approach previously unexplored in the literature. The synergy effect of the SWAF technique has the potential to mitigate a number of limitations related to individual (i.e., conventional water injection and foam flooding) methods encountered in carbonates. In general, carbonate rocks are characterized by a mixed-wet to oil-wet wettability state, which contributes to poor oil recovery. Hence, the smart water solution has been designed to produce a dual-improvement effect of altering carbonate rock wettability towards more water-wet, which preconditions the reservoir and augments the stability of the foam lamellae, which has for some conditions more favorable relative permeability behavior. Then the smart water solution is combined with surfactant (surfactant aqueous solution or SAS) and gas injection produces a synergy effect, which leads to more wettability alteration, and interfacial tension (IFT) reduction, and thus improves the oil recovery. Accordingly, to determine the optimal conditions of smart water solution with an optimal SAS, we conducted a series of experimental laboratory studies. The experimental design is divided into three main steps. At first, the screening process is required so that the candidates can be narrowed down for our designed smart water using the contact angle tests that employ calcite plate (i.e., Indiana limestone or ILS) as the first filter. Following this, the optimum smart water solutions candidates are blended with different types of cationic and anionic surfactants to create optimum SAS formulations. Subsequently, a second screening process is performed with the aim to narrow down the SAS candidates with varying types of gases (i.e., carbon dioxide, CO_2 and nitrogen, N_2) via the aqueous stability test (AST), foamability test (FT), and foam stability test (FST). We employed the state-of-the-art R5 parameter tests for rapid and accurate results in place of the conventional foam half-life method. The most effective combination of SAS and gas candidates are endorsed for the core-flooding experiments. In this work, two types of crude oils (Type A and B) with different total acid and base numbers (TAN and TBN). Results showed that the greatest wettability changes occurred for SW ($MgCl_2$) solution at 3500 (ppm) for both crude oil types. This demonstrates the efficacy of our designed SW in the wettability alteration of carbonates, which is also supported by the zeta-potential measurements. The concentrations of both SW ($MgCl_2$) and CTAB-based surfactants considerably affect the stability of the SAS (i.e., up to 90% foam stability). However when in the presence of crude oil, for the same SAS solution, the foam stability is reduced from 90% to 80%, which indicates the negative effect of crude oil on foam stability. Moreover, the core floods results showed that the $MgCl_2$-foam injection mixture ($MgCl_2$ + CTAB + AOS + N_2) provided the highest residual oil recovery factor of SWAF process of 92% cumulative recovery of original oil in core (OIIC). This showcases the effectiveness of our proposed SWAF technique in oil recovery from carbonate reservoirs. Additionally, changing the large slug of 5 PVs to a small slug of 2 PVs of

smart water solution was more effective in producing higher OIIC recovery and in reducing the fluid circulation costs (i.e., thereby, lowering CO_2 footprint), making the SWAF process environmentally benign. Thus, it is expected that under optimum conditions (SW solution and SAS), the novel SWAF process can be a potentially successful hybrid EOR method for carbonate reservoirs, having both economic and environmental benefits.

Keywords: enhanced oil recovery (EOR); hybrid-EOR; smart water-assisted foam (SWAF) flooding; smart water (SW) injection; foam flooding; carbonates reservoirs

1. Introduction

The hydrocarbon demand and supply continue to occupy a substantial portion of the total energy mix, contributing approximately 85% worldwide [1]. A major part of this portion is dominated by global crude oil demand and supply. According to the International Energy Agency (i.e., IEA, 2020), crude oil supply is estimated to reach around 30% of the world's energy supply by 2035 [1,2]. However, apprehensions regarding climate change have shrunk the likelihood of discovering new colossal oil and gas fields [3], even as the contemporary oil production around the world has become reliant on mature fields [4]. Consequently, enhanced oil recovery (EOR) techniques can be highly potent devices that help retrieve substantial amounts of residual and unswept oil from the prevailing hydrocarbon reservoirs (both sandstones and carbonates). Regardless of the fact that carbonate reservoirs possess 60–65% of the world's unswept oil-proven reserves, indicating highly lucrative prospects (i.e., the economic significance of carbonates reservoirs is enormous) [5–7], the oil recovery from these carbonate rocks is mired with significant challenges. Several relevant studies have stated that globally around 70% of oil reserves in carbonates is inextricable when conventional oil recovery methods are used [8–14]. Carbonate reservoirs are characterized by extremely heterogeneous porosity and permeability, harsh conditions of high-temperature and high-salinity, and mixed-to-oil rock wettability [15–17]. More specifically, the oil-wet carbonate rock causes weakened oil recovery (i.e., low recovery factor or RF) from both the primary methods and water-flooding, when compared to water-wet sandstone rocks [7,8,12–14,18,19]. In oil-wet reservoirs, the oil tends to be located in minuscule pores. When the oil saturation declines, the oil saturation reaches the purported percolation threshold (i.e., number density less than circa 0.3 in a 3D medium) and the oil remains trapped. Being confined to the smaller pores, the amount of oil below the capillary threshold is relatively small. For this reason, conventional water injection is unable to displace all the oil from the pore spaces, and therefore fails to reduce the unswept (bypassed) and residual oil amount in the carbonate reservoirs [7,8,12,18]. Contrary to this, gas injection (e.g., carbon dioxide or CO_2 and nitrogen or N_2) is considered as a good alternative for EOR in carbonate reservoirs [8,12,18]. However, due to their low densities, gases have the propensity for upward movement through the carbonate layers. Hence, during high mobility gas injection, early gas (i.e., CO_2 and N_2) breakthrough [20–22] and reduced volumetric (i.e., macroscopic) sweep efficiency ensue, owing to viscous fingering and gravity override. These are resultant of the adverse effects of unfavorable gas mobility and reservoir heterogeneity in carbonate reservoirs [23]. Injecting slugs of foam-assisted water and alternating gas (FWAG) is a well-established technique that mitigates the heterogeneity issue intensified by the channeling problem, through the use of foam which increases the volumetric sweep efficiency, leading to a reduced gas–oil ratio, and thus augmenting oil production efficiently [22,24–26]. The main limitation of FAWAG injection in carbonate reservoirs is the stability and motion of foam films. Previous studies have generally indicated that oil wetting of rock is a major factor in foam stability and its propagation [20]. The interaction of foam with crude oil in carbonate formation is a significant cause of instability, which causes foam decays [13,19,27,28]. In brief, carbonate reservoirs are prone to: (i) low oil recovery factor (RF), (ii) ineffective water injection due to strong

adsorption of the crude oil on the carbonate rock surface, causing an unstable water film between oil droplets and the carbonate rock surface, and (iii) the foam film ruptures easily when it contacts with crude oil in the carbonate rock.

Thus, as mentioned above, this research paper presents an innovative hybrid EOR technique that coalesces smart water (SW) injection and foam-flooding termed smart water-assisted foam (SWAF) flooding for application in carbonate reservoirs. We have designed the SW solutions to have the characteristic of dual-improvement effects of wettability alteration of carbonate rock and of stabilizing the foam film during the foam flooding stage. This characteristic of the dual improvement effect is resulting in compounded oil displacement. Both the rock–fluid and fluid–fluid interactions are affected by the designed SW solutions. The first effect is improvement in the rock–fluid interaction through surface charge alteration at the rock–fluid interface, causing the change of reservoir rock wettability towards a further water-wet state. The second enhancement effect of the smart water is the modification of fluid–fluid interaction via abating the shielding effect of the electrical double layer (EDL), which improves foam film stability [29–31]. These changes in surface charges at both rock–fluid and fluid–fluid interfaces cause the rock–water interface and the water–oil interface to become of the same sign (i.e., negative or positive charge), creating stable water and foam film, augmenting better EOR (i.e., improved recovery factor or *RF*) [29–32]. Moreover, a synergy effect is generated when the smart water solution is combined with foam flooding via alternating (SAS) and gas (i.e., SAG) injection. By adding surfactant into the smart water (SW) solutions (to generate foam) micro-emulsions form between oil–brine interface producing a synergy effect, resulting in further wettability alteration and interfacial tension (IFT) reduction and helping improve the displacement efficiency i.e., oil recovery. Figure 1 illustrates the injection scheme of the SWAF process, which is comprised of two stages. The first stage is smart water (SW) injection for changing the wettability to become more water-wet by improving the water film stability while simultaneously enhancing the foam lamellae stability as the foam is generated during the second stage. Next, the *SAG* (surfactant aqueous solution alternating gas), is employed to decrease the interfacial tension and improve the displacement efficiency. Furthermore, it should be noted that to date, to the best of our knowledge, there have not been any detailed theoretical nor experimental investigations (i.e., in existing literature) about the coalesced dual improvement effect of wettability alteration and foam stability using smart water in the course of foam flooding in carbonate reservoirs. Thus, to the best of our knowledge, there have been no reported works in the current literature that critically assess the residual oil recovery through the SWAF process in carbonate reservoirs.

It is also worth mentioning that there are other alternatives of EOR technology that expand the envelope of synergy effect in carbonate reservoirs in terms of wettability alteration and IFT reduction. One such alternative technique is nanotechnology for EOR or nano-EOR using nanoparticles (diameter size ranging from 1 to 100 nanometer or nm) [33–39]. One of the key advantages of nano-EOR is wettability alteration (i.e., water film stability) and enhancement of the foam film stability at harsh conditions (high-temperature and high-salinity, or HTHS) in carbonate reservoirs [39–41]. However, compared to our designed smart water, nano-EOR may have the issue of the expense of the nanoparticles and it might run the risk of reservoir damage due to clogging and other environmental concerns. In addition, our designed smart water solution has the advantages of ease of use, effortless availability, ease of injection into the bearing formation, and it can be seamlessly applied in conjunction with other EOR technologies.

Finally, it is also to be noted that this experimental study is a progression of the previous works, viz., [29–31] on an innovative hybrid EOR technique termed smart water-assisted foam (SWAF) flooding for application in carbonate reservoirs. Whereas these preceding studies (SPE-196407-MS) [29–31] mainly focused on the theoretical and modeling aspects (i.e., DLVO theory and surface complexation modeling or SCM). In this study, our focus has been on laboratory experimental facets of the SWAF process in carbonate rocks [20,42].
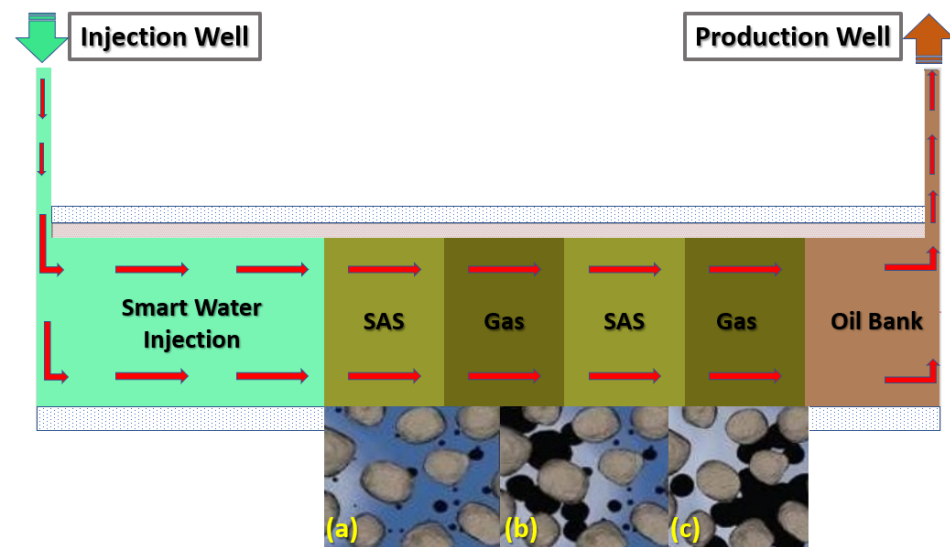
Figure 1. Schematic diagram of SWAF process, which displays the injected scheme scenarios of SWAF method, which starts with smart-water (SW) injection as a secondary mode to change the reservoir wettability (conditioning the reservoir), then the injection of *SAG* (SAS Alternating Gas) i.e., SAS followed by gas injection (i.e., CO_2 and N_2) slugs injections as a tertiary mode or stage. (**a**) Injection of SWAF solution in presence of crude oil, (**b**) SWAF solution interacts with crude oil, and (**c**) oil detaches from rock and moves toward production well.

2. Methodology

This section describes the experimental materials, setup, and the ensuing experimental procedures performed to determine the optimum smart water solutions and optimum SAS formulations for the SWAF process. The optimal conditions can be construed using experimental laboratory studies. The experimental design is divided into three main steps. First, rock wettability measurements using Indiana limestone (ILS) core sample, were obtained by contact angle test. This step aims to select the optimum smart water composition that alters the carbonate rock's wettability towards more water-wet, thereby causing faster oil recoveries. Then the zeta-potential measurements were taken to gain more insights about the crude oil–brine–rock (COBR) interactions (fluid–fluid and fluid–rock interfaces), and thus enable better interpretation of wettability measurement results. In the second step chemical screening (surfactant) was performed, using, (i) an aqueous stability test (AST), (ii) a foamability test (FT), and (iii) a foam stability test (FST). We employed the state-of-the-art R5 parameter tests for rapid and accurate results in place of the conventional foam half-life method. The purpose of the surfactant screening is to establish the conditions that generate a stable foam (i.e., SAS and gas) and reduce the IFT leading to a more stable solution in the absence and presence of crude oil. In this work, two types of crude oils with different total acid numbers (TAN) and total base numbers (TBN), namely, crude oils Type A and Type B. In the third step, after the best smart water solutions and SAS formulations were determined, the core flood tests were conducted. Where the best smart water solutions were dynamically tested through SWAF core-flooding experiments. Conventional water flooding was applied followed by SWAF-injection (i.e., smart water injection and foam flooding). This step aims to determine the ultimate recovery factor under different injection scenarios. With these systematic investigation techniques, the anticipated results are expected to validate the high potential of the SWAF technology for effective enhanced oil recovery from carbonate reservoirs. The flowchart of the systematic experimental design is illustrated in Figure 2.
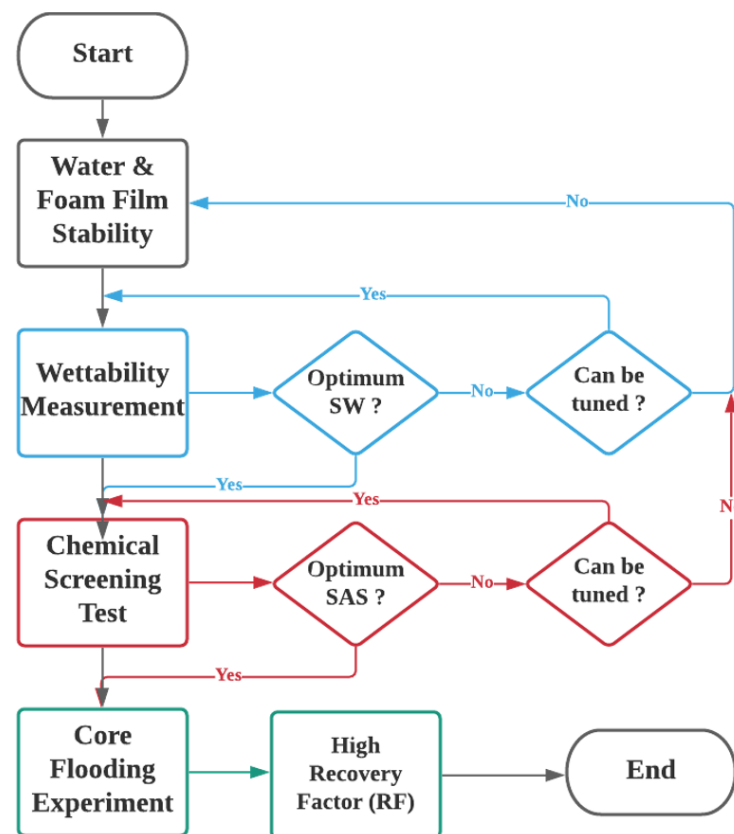
Figure 2. Flow chart of the systematic experimental design used to investigate and optimize smart water-assisted foam (SWAF) flooding process on the laboratory scale. No means "still considering for the best option"; Yes, means "the best option achieved".

2.1. Experimental Materials

The selection of experiment materials to be used for experimental work is the launch of one of the most decisive stages. Any inappropriate selection of the materials may cause deviations from the expected results. Thus, in this study, the materials were carefully selected to generate reliable and representative results.

2.1.1. Core Sample

In this experimental work, the samples used were taken from an outcrop wedge of Indiana limestone (ILS). The ILS is a sedimentary rock, known as Salem-formation, which are quarried largely in the mid-western United States (US) [43,44]. Table 1 shows the ILS core samples' properties in average parameters values (i.e., porosity, permeability, and unconfined compressive strength or *UCS*) as provided by the supplier company (i.e., KOCUREK Industries, Inc., Caldwell, Texas, USA).

Table 1. Properties of the rock as received from the company supplier.

Formation (Type)	Rock Porosity (%)	Rock Permeability (mD)	UCS (psi)	Homogeneous (Yes or No)
Salem	14–19	50–100	4000–5000	Yes

2.1.2. Crude Oil

Two crude oils of Type A and Type B were chosen for this experimental study. The Type A and Type B crude oils are of different compositions with varying total acid numbers (TAN) and total base numbers (TBN). The measured (TAN) and (TBN) results of both types of crude oils (Type A and Type B) along with additional physical properties such as density,

viscosity, sulfur content, and API have been compiled in Table 2. The density and viscosity measurements were gauged at an ambient temperature of 25 °C and reservoir temperature of 80 °C.

Table 2. Crude oils (Type A and Type B) characterization results.

Properties	Unit	Crude-Oil Type A	Crude-Oil Type B
Density at (25 °C)	g/cm^3	0.8848	0.8747
Density at (80 °C)	g/cm^3	0.8694	0.8415
Viscosity at (25 °C)	cP	14.02	10.05
Viscosity at (80 °C)	cP	2.23	1.79
Total Acid Number (TAN)	mg KOH/g	1.17	0.81
Total Base Number (TBN)	mg KOH/g	0.23	0.59
Total Sulfur Content	%	2.51	2.24
API	Degrees	28.42	30.26

2.1.3. Brine Solution

The designed smart water (i.e., ionically modified brine) solutions are prepared carefully based on standard solution preparation procedures. They are synthesized by dissolving a known amount of salts into distilled water at ambient conditions by using a volumetric flask to improve the accuracy of concentration. This section follows the preparation of each solution by weight, volume, and concentrations.

Smart Water Preparation

The designed smart water solutions used in this experimental work were prepared based on standard solution preparation procedures. The ionically modified brine stock solutions were synthesized by mixing the six main salts with deionized water at ambient temperature (25 °C) and atmospheric pressure (1 bar), as shown in Figure 3; a stock solution is a concentrated solution that has to be diluted to some lower concentrated for actual use. The designed smart water solutions are divided into two parts, (i) we varied the concentration of a solution by diluting the salinity of seawater to obtain the optimum salinity, and (ii) we varied the ions in single and binary ionic compound low salinity water at a fixed optimum salinity to examine the effect of single ions and the relative effect of ion in the presence of the other ion. The salinity is fixed at (3500 ppm), which is found to be the model concentration from the first part for the designed smart water solutions. Moreover, the seawater composition used in this experimental work is synthesized based on the typical seawater composition, which has a salinity of 35,000 ppm [45]. It is then further diluted to 5, 10, 20, and 50 times indicated as (Seawater/5), (Seawater/10), (Seawater/20), and (Seawater/50), respectively. To sum up, all brine formulations are tabulated in Table 3. The ionically modified brine stock solutions were further diluted to desired concentrations using the following simple equation;

$$C_1 V_1 = C_2 V_2, \tag{1}$$

where (C_1) is the concentration of the stock solution, (V_1) is the volume from the stock solution, (C_2) is the concentration of the diluted solution, and (V_2) is the volume of the diluted solution.
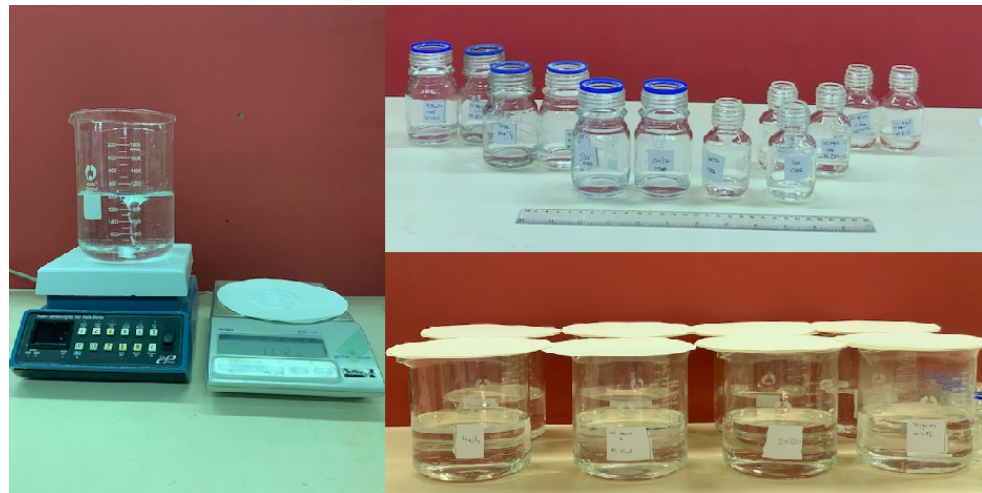
Figure 3. The smart water stock solutions were prepared by mixing controlled amounts of salts with deionized water (at 25 °C and 1 bar); stock solutions were further diluted to 5, 10, 20, and 50 times indicated as (Seawater/5), (Seawater/10), (Seawater/20), and (Seawater/50), respectively.

Table 3. Water-chemistry of synthetic brine solutions used in this experimental work.

Composition	Na^+ (mg/L)	Ca^{2+} (mg/L)	Mg^{2+} (mg/L)	K^+ (mg/L)	$(SO_4)^{2-}$ (mg/L)	$(HCO_3)^-$ (mg/L)	Cl^- (mg/L)	TDS (mg/L)	Ionic Strength (mol/L)	Density @ 25 °C (g/cm³)	Density @ 80 °C (g/cm³)
FW	49,933.0	14,501.0	3248.0	0.0	234.0	0.0	111,947.0	179,863	3.6605	1.1228	1.0949
Seawater	10,669.0	420.0	1330.0	385.0	2730.0	142.0	19,324.0	35000	0.6979	1.0241	0.9988
Seawater/5	2133.8	84.0	266.0	77.0	546.0	28.4	3864.8	7000	0.1396	1.0024	0.9777
Seawater/10	1066.9	42.0	133.0	38.5	273.0	14.2	1932.4	3500	0.0698	1.0003	0.9752
Seawater/20	533.5	21.0	66.5	19.3	136.5	7.1	966.2	1750	0.0349	0.9988	0.9738
Seawater/50	213.4	8.4	26.6	7.7	54.6	2.8	386.5	700	0.0140	0.9979	0.9729
NaCl	1376.9	0.0	0.0	0.0	0.0	0.0	2123.1	3500	0.0599	0.9999	0.9749
CaCl₂	0.0	1264.0	0.0	0.0	0.0	0.0	2236.0	3500	0.0946	1.0002	0.9754
MgCl₂	0.0	0.0	893.7	0.0	0.0	0.0	2606.3	3500	0.1103	1.0002	0.9755
KCl	0.0	0.0	0.0	1835.7	0.0	0.0	1664.3	3500	0.0469	0.9997	0.9747
Na₂SO₄	1133.0	0.0	0.0	0.0	2367.0	0.0	0.0	3500	0.0739	1.0006	0.9761
25% MgCl₂ + 75% NaCl	1032.7	0.0	223.4	0.0	0.0	0.0	2243.9	3500	0.0725	1.0003	0.9751
50% MgCl₂ + 50% NaCl	688.4	0.0	446.8	0.0	0.0	0.0	2364.7	3500	0.0851	1.0004	0.9752
75% MgCl₂ + 25% NaCl	344.2	0.0	670.3	0.0	0.0	0.0	2485.5	3500	0.0977	1.0005	0.9753
25% MgCl₂ + 75% KCl	0.0	0.0	223.4	1376.8	0.0	0.0	1899.8	3500	0.0628	1.0001	0.9751
50% MgCl₂ + 50% KCl	0.0	0.0	446.8	917.8	0.0	0.0	2135.3	3500	0.0786	1.0003	0.9752
75% MgCl₂ + 25% KCl	0.0	0.0	670.3	458.9	0.0	0.0	2370.8	3500	0.0944	1.0004	0.9754
25% MgCl₂ + 75% Na₂SO₄	849.8	0.0	223.4	0.0	1775.3	0.0	651.6	3500	0.0830	1.0008	0.9756
50% MgCl₂ + 50% Na₂SO₄	566.5	0.0	446.8	0.0	1183.5	0.0	1303.2	3500	0.0921	1.0008	0.9756
75% MgCl₂ + 25% Na₂SO₄	283.3	0.0	670.3	0.0	591.8	0.0	1954.8	3500	0.1012	1.0007	0.9756
25% MgCl₂ + 75% CaCl₂	0.0	948.0	223.4	0.0	0.0	0.0	2328.6	3500	0.0985	1.0006	0.9754
50% MgCl₂ + 50% CaCl₂	0.0	632.0	446.8	0.0	0.0	0.0	2421.2	3500	0.1024	1.0006	0.9755
75% MgCl₂ + 25% CaCl₂	0.0	316.0	670.3	0.0	0.0	0.0	2513.8	3500	0.1064	1.0006	0.9755
25% Na₂SO₄ + 75% KCl	1315.9	0.0	0.0	0.0	591.8	0.0	1592.3	3500	0.0634	1.0003	0.9751
50% Na₂SO₄ + 50% KCl	1254.9	0.0	0.0	0.0	1183.5	0.0	1061.6	3500	0.0669	1.0005	0.9753
75% Na₂SO₄ + 25% KCl	1194.0	0.0	0.0	0.0	1775.3	0.0	530.8	3500	0.0704	1.0007	0.9755
25% Na₂SO₄ + 75% KCl	283.3	0.0	0.0	1376.8	591.8	0.0	1248.2	3500	0.0537	1.0001	0.9749
50% Na₂SO₄ + 50% KCl	566.5	0.0	0.0	917.8	1183.5	0.0	832.2	3500	0.0604	1.0004	0.9752
75% Na₂SO₄ + 25% KCl	849.8	0.0	0.0	458.9	1775.3	0.0	416.1	3500	0.0672	1.0006	0.9754
25% Na₂SO₄ + 75% CaCl₂	283.3	948.0	0.0	0.0	591.8	0.0	1677.0	3500	0.0894	1.0006	0.9754
50% Na₂SO₄ + 50% CaCl₂	566.5	632.0	0.0	0.0	1183.5	0.0	1118.0	3500	0.0843	1.0007	0.9755
75% Na₂SO₄ + 25% CaCl₂	849.8	316.0	0.0	0.0	1775.3	0.0	559.0	3500	0.0791	1.0008	0.9755

2.1.4. Surfactant

Four commercial surfactants (i.e., two cationic and two anionic surfactants) were used in total for the experimental study, which are, (i) cetyltrimethylammonium bromide (i.e., CTAB), (ii) dodecyltrimethylammonium bromide (i.e., DTAB), (iii) alpha olefin sulfonate (i.e., AOS), and **(iv)** alkyl ether sulfates (i.e., alpha-foamer), as shown in Table 4. In this experimental work, surfactants were utilized to amend carbonate rock's the wettability, decrease the interfacial tension (IFT), and increase foam film stability, thus improving oil recovery. Two types of gases were studied in this experimental work, viz., CO_2 and N_2.

Table 4. Physical properties of the four (i.e., two cationic and two anionic) surfactants investigated in this experiential study.

Type	CTAB	DTAB	AOS	Alpha-Foamer
Chemical Group	Ammonium Bromide	Ammonium Bromide	Alpha Olefin Sulfonate	Alkyl Ether Sulfates
Formula	C19H42BrN	C15H34BrN	CnH2n-1SO3Na (n= 14–16)	Sodiun C12-C14 Layreth Sulfate
Form at 25 °C	White powder	White powder	Liquid	Liquid
Boiling Point, [°C]	235	239	100	88
Flash Point, [°C]	244	246	>94	28
Specific Gravity at 25 °C, [-]	1.11	1.05	1.06	1.03
Density at 25 °C, [g/cm^3]	1.11	1.05	1.06	1.03
Molecular Weight. [g/mole]	364.45	308.34	315.00	<300.00
Viscosity at 25 °C, [cp]	[-]	[-]	122.00	20.00
CMC, [mg/L]	346 [1 mM]	4200 [14 mM]	301.00	2.20
Surface Tension (SFT), [mN/m]	31.7	49.1	31.6	29.9

2.1.5. Gas

Two types of gases were investigated in this experimental study, viz., nitrogen (i.e., N_2) and carbon dioxide (i.e., CO_2). CO_2, unlike natural gas, has a positive effect through reduced carbon footprint. Thus, using CO_2 can be potentially more lucrative in both economic and environmental terms since, economically, trade and export of natural gas may be more viable than utilizing it for injection in the oil reservoirs. Subsequently, nitrogen (N_2) gas of purity 99.98% was used to perform the core-flooding experiments.

2.2. Experimental Procedure

In this section, we detail the experimental procedures conducted using the SWAF process to realize the set objectives for this experimental work. These set objectives are as follows;

- To identify SWAF's optimum condition i.e., the best smart water (SW) that achieves the highest wettability modification by tuning the water chemistry (i.e., ion type, concentration, salinity).
- To generate SAS that will ultimately reduce the interfacial tension (IFT) and has high foam stability in presence of crude oil.
- To investigate the proposed hybrid technique in the dynamic mode in which different core flooding scenarios are employed towards the highest recovery factor.

2.2.1. Compatibility Test

A compatibility test between injected fluid (e.g., our designed smart water) and formation water (FW) is a crucial screening step that thwarts precipitation (i.e., forming of sediment) and any formation damage that could occur to palpably reduce the oil production [46,47].

Therefore, during the course of the experimental trials, all those designed SW solutions that were incompatible with our selected FW were excluded from the subsequent laboratory analyses. The samples of SW solutions blended with FW were placed in the oven for 48 h at (80 °C), and the after-effect was observed [20].

2.2.2. Wettability Measurement

Wettability is considered a vital parameter for hydrocarbon recovery. Permanent reservoir damage could occur if the wettability of the reservoir is not properly been identified [48]. Wettability is the proclivity of solid to adhere to one fluid rather than another fluid present [48]. The fluid attaches to the solid surface forming a contact angle between the wetting liquid and the solid surface. The wettability of a reservoir is established using the contact angle measurement of the tangent from the rock surface to the wetting droplet across the denser fluid. Figure 4 illustrates the contact angle for different systems (i.e., oil-wet and water-wet states.
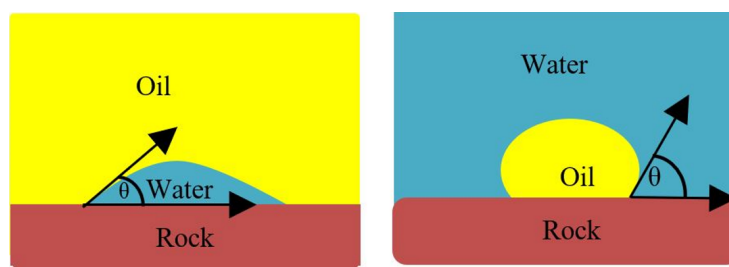
Figure 4. Sessile drop method; If $\theta < 90°$, the system is water-wet; and if $\theta > 90°$, the system is oil-wet.

According to Chilingar and Yen [49], contact angles suggesting types of wettability for carbonate reservoirs are listed in Table 5.

Table 5. Wettability classification of carbonate reservoirs.

Contact Angle	Wettability
0° to 80°	Water-Wet
80° to 100°	Intermediate Wettability
100° to 160°	Oil-Wet
160° to 180°	Strongly Oil-Wet

In carbonate rocks, the reservoir rock's initial water-wet condition is changed to the oil-wet state by the polar constituent being adsorbed in crude oil or via the deposition of a thick organic layer of crude oil on rock surface [50]. The injected EOR fluids are able to replace the oil from the rock surface, which leads to the oil occupies into the larger pore spaces altering the rock wettability of carbonate rock toward water-wet state [50].

Contact Angle Test (CAT)

Following the compatibility test between injected fluid (e.g., our designed smart water) and formation water (FW), the selected smart water (SW) solutions from the compatibility test were employed in wettability-measurement using contact angle test (CAT). For this study, the contact angle measurement was performed utilizing the Sessile drop-down technique [51–53] (i.e., by using IFT 700 set-up) to investigate the effect of SW on carbonate rocks in terms of wettability alteration (i.e., for selecting the optimum SW solutions). Firstly, the model salinity of the designed SW solutions was screened out from the synthetic seawater dilution, which was succeeded by single and binary ionic compounds SW that had fixed model salinity. The process of the Sessile down method was performed in conformity to existing literature [54–56]. Additionally, this procedure was executed (repeated) twice in order to ensure the consistency of the wettability measurement test. One should note that the average of the contact angles was taken as the final contact angle for each particular time interval of 0, 24, and 48 h at 80 °C. Smart water (SW) solutions with the maximum and minimum alterations in contact angles for both diluted and ionically modified low salinity brine groups were then shortlisted to advance for chemical screening tests [20].

Core Slices Preparation

For the contact angle measurement test, the core plug was sliced into 2 cm length slices having 2 cm width, and 3–5 mm thickness to fit the IFT-700 equipment for contact angle measurement. Then the core slices were smoothed for an even surface, which is required for contact angle measurement. Moreover, core sample slices are cleaned with methanol and toluene to remove the possible existing salts, crude oil, and other deposits from core sample slices, as shown on the right side of Figure 5. Then these polished core slices are oven-dried at 9080 °C for 24 h. On the dried core slices, the water droplet is vertically dropped as shown in the left side of Figure 5, to ascertain the water-wet condition of core slices prior to saturating them with formation water using vacuum pump desiccator, which

produces an initial water state for test. Once no more air bubbles are released from the core slices, signifying complete saturation of the core slices with formation water, the saturation process is over. Subsequently, the saturated core slices submerged in formation water are oven-dried at 80 °C for 3 days, after which the core slices are removed from formation water and allowed to air dry. The dried core slices are aged by placing them into crude oil in the oven at 80 °C for 5 days to create oil-wet core slices. Then at last, after 5 days the core slices are removed from crude oil, cleaned with distilled water, and air-dried beforehand for the wettability measurements.

Figure 5. Indiana limestone (ILS) core sample slices are cleaned with methanol and toluene to remove possible existing salts, crude oil, and other deposits (**right**); core sample slices are in a hydrophilic (water-wet) state (**left**).

Contact Angle Test on Treated Core Slices

After the treated core sample slice was (i) aged with crude oil at (80 °C) for five full days, and (ii) taken out from crude oil and rinsed with distilled water and dried out, then the treated core sample slice is carefully placed in (IFT-700) cell. The wettability measurement process starts with letting a droplet of water fall on the treated core sample slice and the angle between solid rock surface and tangent of water from the solid surface is recorded as the initial contact angle [57]. The treated core sample slice is treated with synthetic seawater (35 ppm) at (80 °C) before subsequent contact angle is carried out for every 24 h up to 48 h. Then, the core sample slice is rinsed with distilled water whenever removed from the synthetic seawater solution. The same procedure is applied for each seawater dilution and ionically modified low salinity waters (i.e., our designed smart water solutions). The contact angle measurement's procedure is similar to the existing literature [54–56]. Moreover, this process (i.e., procedure) was performed in double (and triple) repeats to ensure the reliability of the contact angle test (i.e., see Appendix A). Finally, an average of the contact angles is taken as the concluded contact angle for each specific time interval of 0, 24, and 48 h. Figure 6 displays contact angle measurement was carried out by applying IFT-700.
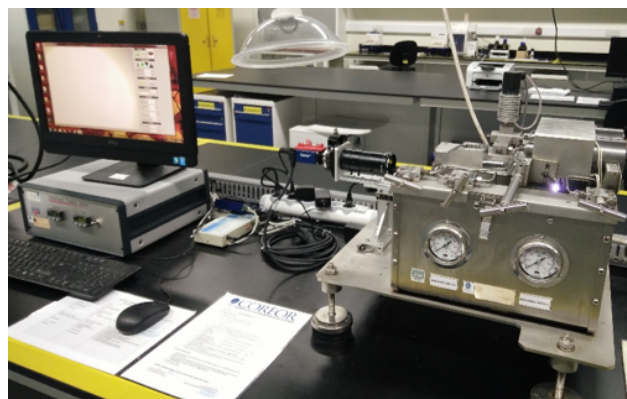
Figure 6. Interfacial tension meter (IFT 700) setting for measuring the contact angle (CA).

2.2.3. Zeta Potential (ZP) Measurements

During smart water/low salinity (ionically modified brine) injection, one of the key mechanisms underlying wettability change of the oil-wet carbonate rocks is the electrical charges of crude oil/brine/rock (COBR) system (i.e., surface charge alteration). Thus, to measure the surface potential at COBR interfaces, the surface potential or zeta potential (ZP) measurements were performed at one bar (atmospheric) pressure and 80 °C temperature. In this work, the ZP measurements (i.e., at the shear plane) were performed by using two measurements devices, namely, Zeta-sizer (SZ-100) and Zeta-check (Particle Matrix GmbH). Both ZP devices use the electrophoresis method to measure surface potential (zeta potential). The electrophoresis method can measure a wide range of zeta potentials (i.e., from −2000 mV to +2000 mV). Besides, the temperature limit of 100 °C makes it possible to measure surface potential at reservoir conditions (80 °C).

Zeta Potential Test (SPT) on Treated Core Sample Powder

The Indiana limestone (ILS) core sample slices are prepared by first milled into a powder. To recreate authentic reservoir environments, the limestone particles were saturated in formation water (FW) at 80 °C for 3 days for the carbonate rock surface to form a water-wet or water film. After this the limestone particles are removed from the formation water (FW). Then, 0.2 g of water-wet limestone particles are dissolved in a 20 mL solution of smart water (SW) to obtain an aqueous solution of 1 wt%. These samples are oven-dried for 48 h at 80 °C. Additionally, a crude oil in brine sample is made by combining 2 mL of crude oil with 10 mL of each brine sample according to the volumetric ratio of 1:5. These samples are placed in the oven for 48 h at 80 °C. It is worth mentioning that weight in percent of limestone particles in brines and volumetric ratio of crude oil in brines are derived from earlier published literature [58]. Furthermore, an ultrasonic bath is used for sonicating all prepared samples, prior to running zeta potential measurements, so that suspension and emulsion solutions can be generated. To gauge the cloudiness of sample solutions a finger is placed behind the solution and the finger should appear blurry yet identifiable [59]. Once the selected samples are ready, they are positioned into the ZP apparatus (e.g., Zeta-sizer/SZ-100 or the Zeta-check/Particle Matrix GmbH), as provided in Figure 7. The temperature is set at 80 °C, and the results are noted once the temperature is steady. Lastly, the average of three measurements at the shear plane was selected as the anticipated surface potential value.

Figure 7. Zeta potential (ZP) measurements; Zeta-sizer (SZ-100) (**bottom left**), the ultrasonic bath (**top left**), and Zeta-check (Particle Matrix GmbH) (**right**).

2.2.4. Aqueous Stability Test (AST)

The key objective of chemical screening tests (i.e., surfactant screening) is the eventual creation of a stable foam that leads to reduced interfacial tension (IFT) and forms surfactant aqueous solutions (FW) of higher stability in the presence of the selected crude oils. The FW preparations were primed by using varying proportions of four-type of surfactants, namely, CTAB, DTAB, AOS, and alpha-foamer to the chosen smart water (SW) solutions. Initially,

surfactant screening was conducted through the aqueous stability test (AST). The definitive aim of the *AST* is to derive the smart water (SW) solutions that form with each of the four types of selected surfactants (CTAB, DTAB, AOS, and Alpha-foamer), a stable and transparent (clear) FW at a temperature of 80 °C. If precipitates are formed in the solution, the pore throats of the reservoir rocks may be obstructed or a non-uniform distribution can occur, which results in unproductive oil recovery or reservoir rock damage. For our investigations, the aqueous stability test (*AST*) was carried out in the following steps, (i) first, small 10 ml test tubes were cleaned and dried in the oven, (ii) then, to prepare samples of FW, surfactants from stock solutions were mixed to each smart water (SW) and formation water (FW) by employing a mechanical micropipette; and as mentioned earlier, it was based on the specific solution computation, (iii) next, the empirical results were recorded at room temperature, (iv) after this, the test tubes were placed in the oven at 80 °C, and (v) at the end, the results were confirmed and logged after each 0, 6, 12, 24, 48, and 72 h, at temperatures of 25 °C and 80 °C. The optimal formulation is a clear (transparent) solution, whereas those that formed precipitates at the bottom of the tubes or cloudy solutions all through the tubes are deemed as the least stable FW formulations [20].

2.2.5. Foamability and Foam Stability Test (FT/FST)

Foam stability is usually encountered in many industrial processes and everyday life phenomena; nevertheless, there exists neither a general theory explaining the mechanism of their stability nor a generally accepted test that facilitates a reliable determination and evaluation of foams formed by different types of surfactants [60]. This is due to the fact that foam is a challenging liquid–gas dispersed system whose properties are characterized by non-equilibrium adsorption coverage at liquid–gas interfaces [61]. In this study, our evaluations to characterize the foamability and foam stability of the surfactant aqueous solutions have been conducted via a rapid and incisive pneumatic test called the R5 parameter. The R5 parameter is described by the ratio of the relative foam height after a five minutes duration to the initial foam height [60,62]. Additionally, the variations in R5 parameter values with changes in surfactant concentrations correspond to those of foam half-life with surfactant concentration. Thus, instead of gauging for prolonged hours for the foam half-life, an equivalent data can be obtained using the R5 parameter test which needs only a few minutes to complete. Furthermore, with the R5 parameter test, specifics about the solution contents of foams can be acquired. Additionally, this parameter can be set as a criterion for the assessment of foam stability [60,62]. The key benefits of the proposed R5 parameter test are given below [60]:

- The test is easy, quick, and convenient, and the measurements are reasonably repeatable.
- During the test, the amount (volume) of gas used to make the foam is precisely regulated.
- The R5 parameter can be used to acquire similar details about foam stability akin to the prolonged measurements taken of the foam halftime in the half-life method. Foam stability is indicated by R5 values greater than 50%.
- It is easy to determine the solution content of a foam and use it as an additional parameter to classify foams.
- The method can be applied to all kinds of foams, including transient ("wet foams") and metastable ("dry foams"), allowing for a reasonable comparison of different types of foams.

Figure 8 displays the foamability and foam stability setup used to generate the required foam. For the foamability and foam stability experiments, FW (i.e., 12.5 mL at the height of 86 cm) were poured into glass columns. Then, with the aid of a syringe, fifty (50 mL) and twenty-five (25 mL) of gas (N_2 or CO_2) were manually introduced into FW within the first 20 s (i.e., average volumetric rate of 4.5 and 9.0 L per hour). Following the gas injection, the valve (stop-cock) connecting the column with the syringe was immediately closed. Hereafter, the initial foam and FW heights were measured. Foam heights and FW level were then measured again at five (5) minutes intervals to determine the R5 parameter. Moreover, the foamability and foam stability tests were conducted for each

selected surfactant at different concentrations in the absence and presence of crude oils (Type A and Type B). Finally, the most effective FW (in combination with the most effective gas type) were determined and their foamability and foam stability were further studied at different smart water (SW) solutions with different salinity levels and in the presence of crude oils (Type A and Type B) [20].
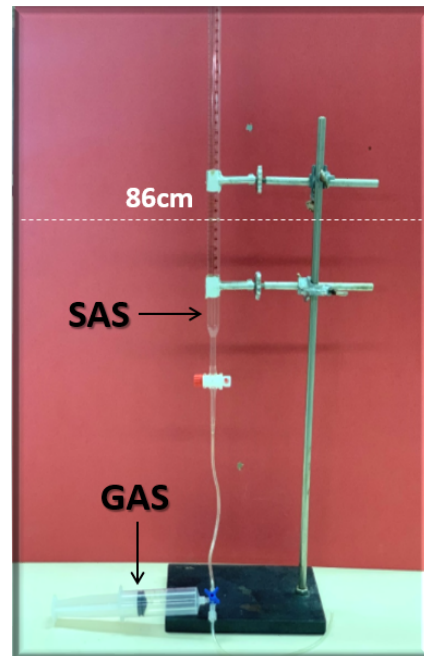
Figure 8. Foamability and foam stability set-up using the R5 parameter, which is defined as the ratio of foam-height at five-minutes to initial foam height.

2.2.6. Core Flooding Test (CFT)

All the apparatus needed for the core flood experiment are thoroughly cleaned before commencing experiments, which include pumps, core sample holders, sleeves, accumulators, tubing, and crude oil collectors. Then the required rates of water, injection and production pressures, and profile of differential-pressure transducer were logged onto the data logger system of the Core-flooding Scheme (CFS-830-Z) unit, which is illustrated in Figure 9. The core-flooding experiments were performed with a confining pressure of 2700 psi and back pressure of 2300 psi. Besides, an integrated part of the (CFS-830-Z)unit system is the smart-flood software and computer data acquisition and control system hardware, which provides real-time (on-time) monitoring of all measured values (e.g., volume, temperature, and pressure, etc.). Moreover, the system (CFS-830-Z) unit contains three accumulators (1, 2, and 3) used to host the injection fluids as shown in Figure 9. In the case of SWAF injection, we have five fluids, viz., formation water (FW), smart water (SW), surfactant aqueous solution (FW), gas, and crude oil) in which we split them into two main groups or stages. In the first stage, we filled the three accumulators with formation water, smart water, and crude oil (i.e., which simulate the primary and secondary oil recovery phases). We keep the crude oil in the same accumulator during the second stage, and we fill the other two with FW and gas (i.e., which represent the tertiary oil recovery phase). These fluids were pumped inside the core sample using a dual cylinder positive displacement pump displacing fluid at desired injection rate (e.g., 0.2 cubic centimeter or cc per minute). To save the pump from the corrosive fluid (such as high salinity brines), we pumped distilled water to the bottom of any of the three accumulators filled with our five injected fluids (formation water, smart water, SAS, gas, and crude oil) to transfer these fluids to the carbonate rock core sample. The confining, pore, inlet, and outlet pressures were measured with pressure transducers, and then the differential pressure across and along the carbonate rock core sample was measured with various differential pressure transducers (i.e., see

Figure 9). Moreover, gas is displaced from a pressured (e.g., N_2) cylinder connected to the system (CFS-830-Z) unit where the gas flow is controlled and measured through an inlet and outlet accumulator's regulators that filled with gas. Finally, production fluids (e.g., crude oil, water) are collected in graded tubes mounted in a timely set fraction collector (e.g., crude oil collector) [20].
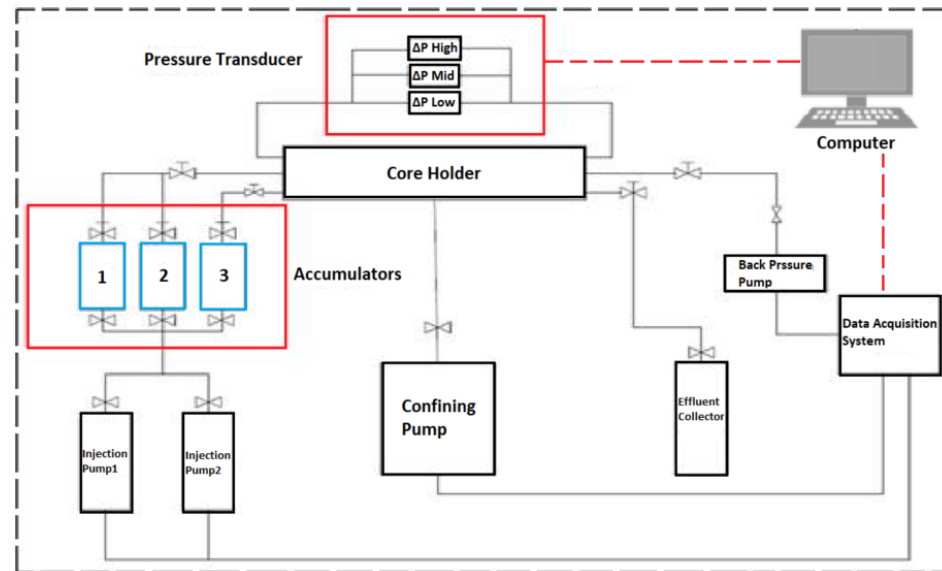
Figure 9. The Core-flooding System Unit (i.e., CFS-830-Z, King Abdulaziz City for Science and Technology, KACST, Saudi Arabia).

Core Sample Preparation and Saturation

Cylindrical ILS core samples were prepared (see Figure 10) and dried overnight in an oven at (80 °C). The dimension (3.82 cm diameter × 7.66 cm length) and dry weight of the selected core samples were measured and recorded . Hereafter, the core samples were placed in a desiccator where a vacuum pump was applied for 72 h as an aging time to ensure that no more gas bubbles are observed. When appropriate vacuum pressure was reached, the ILS core sample was saturated using a synthetic FW solution. After saturation, the core sample was weighed and its dry and wet weight and the brine density were used as the pore volume (PV), and hence the ILS core sample porosity (i.e., approximately 19%). Table 6 shows the Indiana Limestone (ILS) core-samples properties (e.g., porosity, permeability, and Unconfined Compressive Strength or UCS) given by the supplier company (i.e., KOCUREK Industries Inc., Caldwell, Texas, USA) as an average values parameters. The core-sample were cut to (shorter) pieces, and their properties were measured again to obtain more accurate core-sample's characterization, as shown in Table 7.

Table 6. Average properties of Indiana limestone (ILS) core sample as received from the company supplier (KOCUREK Industries Inc., Caldwell, Texas, USA).

Formation (Type)	Permeability (mD)	Porosity (%)	Length (cm)	Diameter (cm)	Area (cm^2)	Bulk Volume (cm^3)
Salem	50–100	14–19	30.48	3.81	11.40	347.50
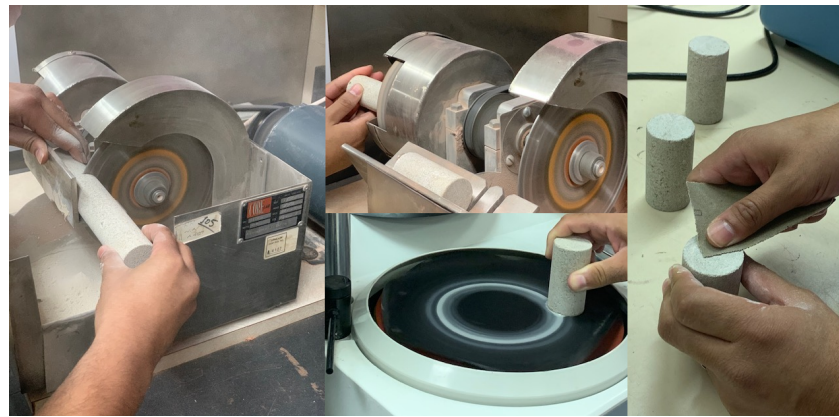
Figure 10. Indiana limestone (ILS) core sample preparation procedures using geological cutter machine, polisher, and sandpaper preparation.

Table 7. Indiana Limestone (ILS) Core-sample Petrophysical Properties.

Core-Sample (Number)	Permeability (mD)	Porosity (Gas)	Length (cm)	Diameter (cm)	Area (cm²)	Bulk Volume (cm³)	Dray-Weight (gram)	Wet-Weight (gram)	Pore Volume (PV in cm³)	Porosity (Saturation)
1	50–100	19.40	7.66	3.82	11.46	87.79	191.51	208.31	16.79	0.1912
2	50–100	18.30	7.30	3.82	11.46	83.66	182.04	197.72	15.67	0.1873
3	50–100	18.50	7.35	3.82	11.46	84.24	184.61	200.10	15.48	0.1838
4	50–100	17.93	7.32	3.82	11.46	83.89	183.92	199.25	15.32	0.1826
5	50–100	15.85	7.33	3.82	11.46	84.01	184.27	197.25	12.97	0.1544
6	50–100	17.94	7.48	3.82	11.46	85.73	189.73	204.88	15.14	0.1766
7	50–100	17.59	7.40	3.82	11.46	84.81	190.88	205.76	14.87	0.1753
8	50–100	14.71	7.45	3.82	11.46	85.38	189.72	202.14	12.41	0.1454
9	50–100	15.30	7.50	3.82	11.46	85.96	190.96	204.61	13.64	0.1608
10	50–100	16.20	7.49	3.82	11.46	85.84	190.95	205.19	14.23	0.1658

Mineralogy Analysis

X-ray fluorescence (XRF) and X-ray diffraction (XRD) were applied to identify the component minerals of the Indiana limestone (ILS), and thus provide a better understanding of the reactions and interactions of our specific COBR system (i.e., the interactions between brine–crude oil and brine–rock interfaces). X-ray fluorescence (XRF) analyses the components (i.e., ion type) present in the rock core sample, whereas X-ray diffraction (XRD) determines the rock core samples' possible mineralogy. This can double confirm the actual mineral content that existed in the rock sample and provide a more complete and accurate mineral characterization of the Indiana limestone (ILS) core sample. Finally, the acquired data from XRD was processed for identification of different minerals sorted according to their respective diffraction angle or identification-2θ (X-access) and intensity or quantification (Y-access) on a diffraction pattern curve as shown in Figure 11.
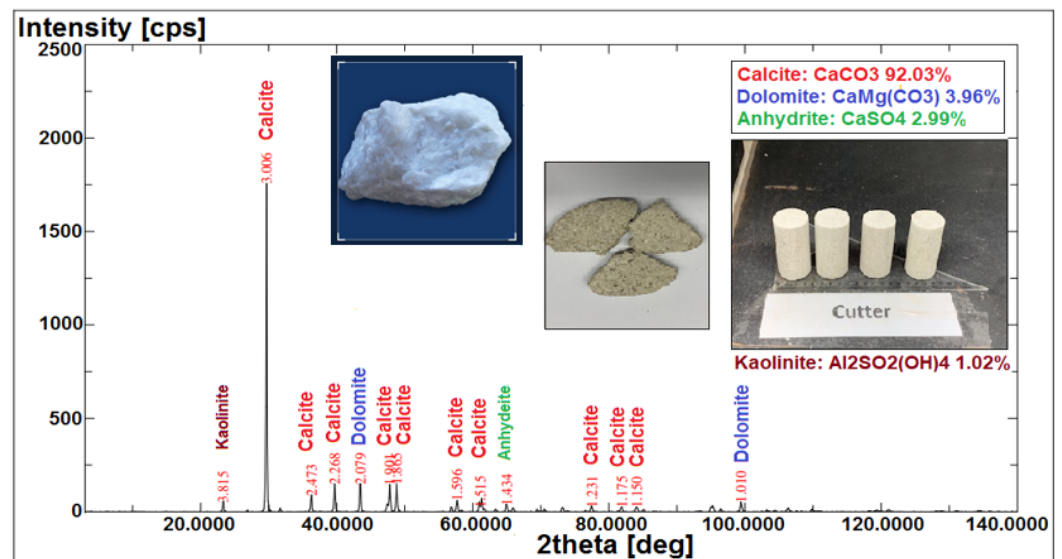
Figure 11. Qualitative analysis of minerals in Indiana limestone (ILS) using XRF and XRD analysis.

Permeability Measurement

The saturated ILS core sample (with synthetic formation water) was then placed in the core sample holder (i.e., see Figure 9) of the Core-flooding System (CFS-830-Z) unit, and confining pressure of 2700 psi and backpressure of 2300 psi were applied. Crude oil, synthetic seawater, smart water (SW) solutions, surfactant aqueous solution (SAS), and gas were poured into the accumulators (i.e., since we have only three accumulators and five injected fluids, we implemented this step in two stages), and all line connections were tightened. The ILS core sample was flooded with seawater solutions (i.e., open the valve of the accumulator that filled with synthetic seawater solution) at different flow rates (e.g., 0.2, 0.4, 0.6, 0.8, and 1.0 cubic centimeter per minute (cc/min) and the pressure drop across the core sample was recorded for each flow rate. Finally, Darcy's law was applied to calculate the absolute permeability.

Crude Oil Flooding (i.e., Drainage Process)

After that the porosity and the permeability of the ILS core sample were calculated, the crude oil process was started by injecting crude oil (i.e., open the valve of the accumulator that filled with crude oil) into the saturated ILS core sample. This step was done at a flow rate of 0.2 cc/min until water production ends. The initial water saturation or S_{wi}, initial oil saturation (S_{oi}), and original oil in core (OOIC) were then determined by applying a material balance, and the end effective oil permeability (K_o) was calculated using Darcy's law. The core sample was left for wettability restoration and crude oil-water distributions refinement at the pore level. At this stage the ILS core sample was ready for seawater and smart water (SW) injection, and SAS (surfactant aqueous solution) alternating gas (SAG) flooding.

Sea Water Flooding (i.e., Imbibition Process)

The seawater injection started at 0.2 cc/min and continued to residual oil saturation (S_{so}). The produced oil productions samples were collected in graded tubes and pressure drop was monitored through the data logger system (i.e., main controller monitor screen). This step was to continue until no more oil was produced at two pore volumes (2 PV). The effective water permeability (K_{we}) was then calculated by applying Darcy's law. The oil recovery and post-secondary (conditioning the core sample) seawater flooding residual oil saturation (S_{or}) were determined via a material balance.

Smart Water (SW) Flooding (i.e., Imbibition Process)

The smart water (SW) injection started at 0.2 cc/min and continued to residual oil saturation (S_{so}). The produced oil productions samples were collected in tubes and the pressure drop was monitored through the data logger system (i.e., main controller monitor screen). This step was continued until the two pore volumes (2 PV) was reached.

SAS Alternating Gas (SAG) Flooding

After injection of two pore volumes (2 PV) of smart water (SW) solutions, SAS (surfactant aqueous solution) alternating gas or (SAG) flooding was started at 0.2 cc/min and continues to residual oil saturation (S_{so}). This injection step consisted of injecting 0.5 PV of SAS followed by 0.5 PV of gas, and SAS alternating gas was repeated once (e.g., a total of 2 PV), so-called scenario 1, as shown in Figure 12; scenario 2 consisted of injecting 1 PV of SAS followed by 1 PV of gas; scenario 3 consisted of injecting 0.5 PV of gas followed by 0.5 PV of SAS, and gas alternating SAS was repeated once (e.g., Total of 2 PV). Finally, Scenario 4 consisted of injecting 1 PV of gas followed by 1 PV of (SAS) or surfactant aqueous solution.
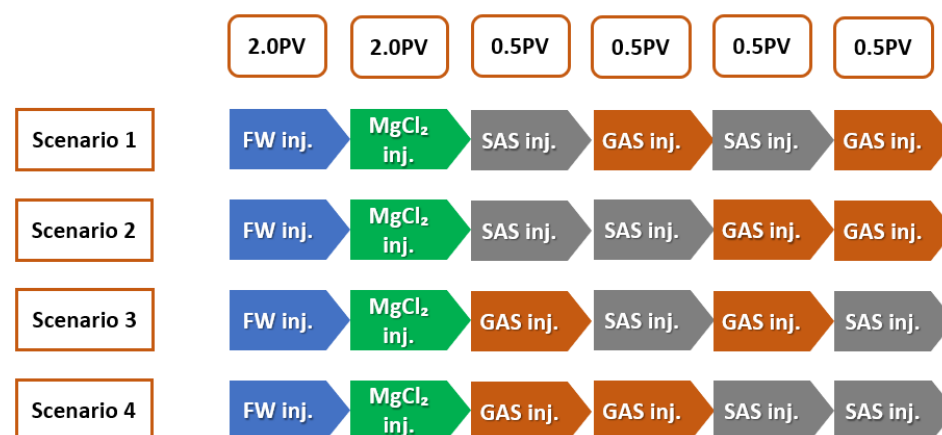
Figure 12. SWAF injection Scenarios ($MgCl_2$ + Oil Type-A); the effect of crude oil type (Type-A and Type-B) at different smart-water (*SW*) solutions.

In summary, Figure 12 illustrates the injection scenarios of smart water-assisted foam (SWAF) flooding or SWAF process. Scenario 1 starts with two (2) pore volumes (2 PV) of formation water injection. Then, the two pore volumes (2 PV) of smart water (SW) injection alter the carbonate rock wettability towards a more hydrophilic (water-wet) state. Hereafter, we inject two pore volumes (2 PV) of SAG or SAS (surfactant aqueous solution) alternating gas, which is divided into 0.5 PV SAS, 0.5 PV gas, 0.5 PV SAS, and 0.5 PV gas. Scenario 2 consisted of injecting (1 PV) of SAS followed by (1 PV) of gas. Scenario 3 consisted of injecting (0.5 PV) of gas followed by (0.5 PV) of SAS, and gas alternating (SAS) was repeated once (e.g., Total of 2 PV). Finally, scenario 4 consisted of injecting (1 PV) of gas followed by (1 PV) of SAS.

3. Experimental Results and Discussions

3.1. Compatibility Test

After synthetic formation water (FW) or connate water is prepared (i.e., to establish initial water saturation of our carbonate core sample [63]), we mixed it with our designed smart water (SW) solutions and kept the mixed solutions in the oven for 48 h at 80 °C. Precipitation was observed for formation water (FW) mixed with sodium bicarbonate, which has 2542.2 ppm of HCO_3. Consequently, sodium bicarbonate was excluded in the subsequent tests. Slight precipitation was also observed on formation water (FW) mixed with seawater which has 142 ppm of HCO_3 and no precipitation was observed for other low salinity waters. The outcome of the compatibility test can be seen in Figure 13.
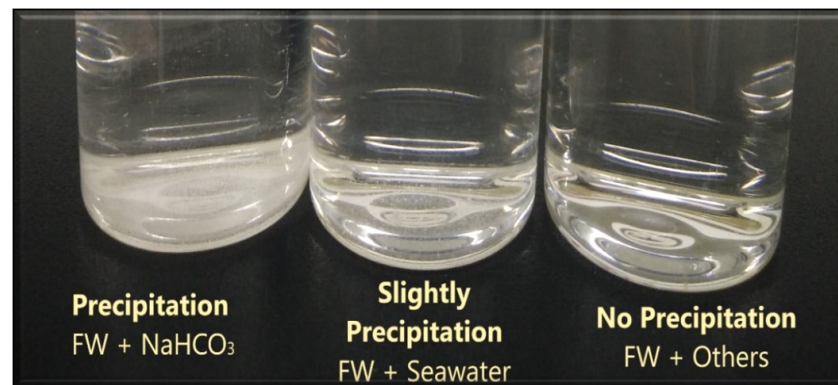
Figure 13. The results of the compatibility test (*CT*) between synthetic formation water and our designed smart water (SW) solutions.

3.2. Wettability Measurement

The ultimate goal of this wettability measurement is to select the optimum designed smart water solutions that reduce the contact angle the most, and thus shift the carbonate wettability rock towards a more water-wet condition, as discussed earlier in Section 2.2.1. Moreover, the total averaged reduced contact angle of each low salinity water solution (i.e., LSWs or our designed smart water solutions) is illustrated in the bar chart in Figures 14–22.

3.2.1. Seawater Solution and its Dilutions

Figure 14 displays the total cumulative reduction of contact angle after 24 h and 48 h in the presence of seawater and its dilution. One should note that after 48 h no pronounced changes in the results of the contact angle measurements were detected. The results evince that seawater was unsuccessful in altering the contact angle even after 48 h had elapsed. The decreased salinity levels to 7000 ppm, 3500 ppm, 1750 ppm, and 700 ppm led to improved contact angle reductions. The reduced contact angle shows that lowering the salinity level was able to shift the wettability of limestone core sample slices towards more water-wet, and has the potential to improve oil recovery. This trend of the results is in agreement with previous studies [64–66]. Interestingly, it was found that the dilution of seawater (1750 ppm) is the optimum salinity level where the highest change in wettability was observed, and further diluting the water resulted in a lower change in contact angle. We observed that the 20-times diluted seawater (1750 ppm) has a total of 14.4° contact angle change and 50-times diluted seawater (700 ppm) has a total of 4.3° contact angle change. This might be due to the reduction in potential determining ions in the designed smart water (SW) solutions with further dilution as mentioned by Fathi and co-workers [67–69]. A similar trend of results was also acquired by Su and co-authors [70] who concluded an optimum salinity level for maximum wettability alteration to happen.
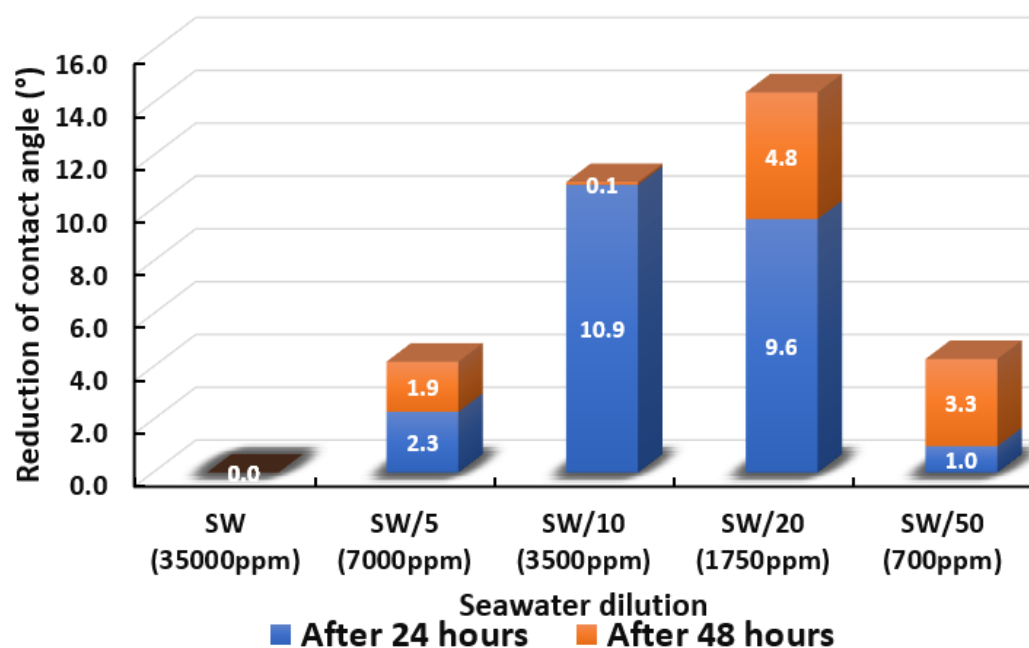
Figure 14. Contact angle reduction results for seawater dilution. It should be noted that SW, SW/5, SW/10, SW/20, and SW/50 representing Seawater, Seawater/5, Seawater/10, Seawater/20, and Seawater/50 respectively.

3.2.2. Single Ionic Compounds Smart Water Solutions (3500 ppm)

Figure 15 displays the total reduced contact angle of Indiana limestone (ILS) in the presence of single ionic compound low salinity water. It is observed that $MgCl_2$ has the most remarkable ability to shift contact angle close to the water-wet state. $MgCl_2$ reduces $6.7°$ of contact angle in total. The initial 24 h has a more significant impact on contact angle change. However, this was not followed by Na_2SO_4, which changed the total contact angle to $4.7°$ after 48 h. Thus, from the results it is evident that $MgCl_2$ is a better wettability alteration modifier than Na_2SO_4 and this finding concurs with the work from Karimi and co-authors [71,72] and Gomari and co-workers [73]. Furthermore, when the impact of $CaCl_2$ is compared with that of Na_2SO_4 in causing wettability improvement towards more water-wet for ILS core sample slices, we observed that $CaCl_2$ has slightly reduced capability. The total contact angle reduction was $3.5°$ after 24 h and no modifications were found even after 48 h had elapsed. Similar results were observed for NaCl and KCl, which have the least impact on contact angle alteration in ILS core sample slices. Besides, NaCl and KCl were only able to reduce the total contact angle of $1.4°$ and $1.3°$, respectively. Additionally, a higher change in contact angle was found when our designed smart water (SW) solutions containing divalent ions rather than monovalent ions [31]. These results are also consistent with other research implying that magnesium (Mg^{2+}) ion, calcium (Mg^{2+}) ion, and sulphate (SO_4^{2-}) ion are the potential determining ions ($PDIs$) for the low salinity water (LSW) effect in carbonate rocks [54,67–69,74–77].

In summary, single ionic compounds smart water (SW) solutions containing divalent (e.g., Mg^{2+}, Ca^{2+}, and SO_4^{2-}) ions are more capable of reducing the contact angle of Indiana limestone (ILS) compared to single ionic compounds smart water (SW) solutions containing monovalent (e.g., Na^+, K^+) ion, which alter the rock wettability of ILS towards the more water-wet state. Consequently, this allows for easier detachment of crude oil from the surface of carbonate rocks (i.e., ILS).
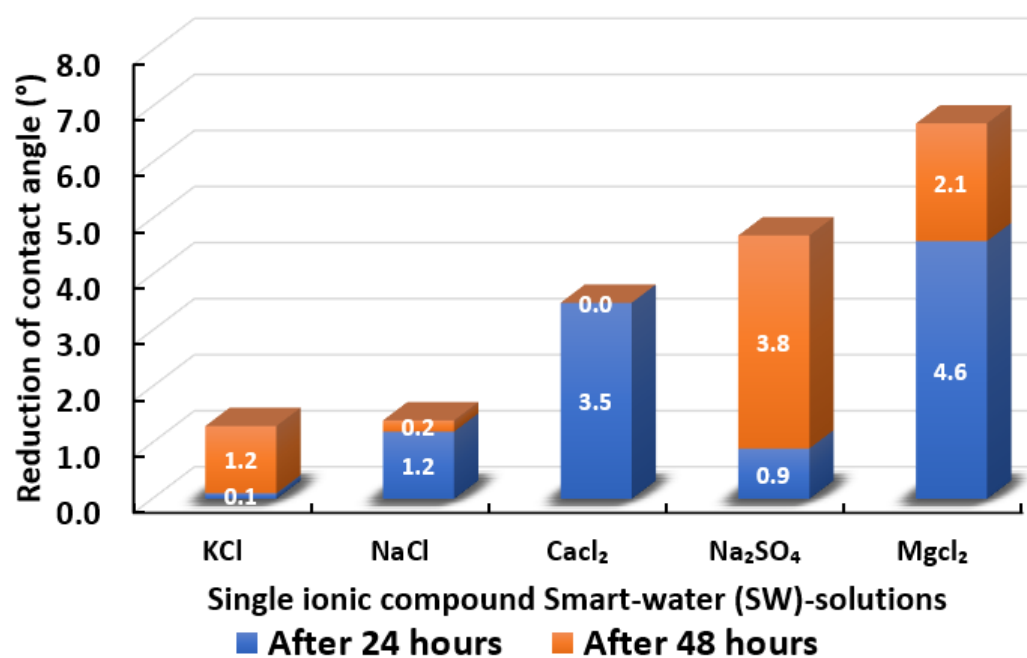
Figure 15. Contact angle reduction results for single ionic compounds smart water (SW) solutions (3500 ppm).

3.2.3. Binary Ionic Compounds Smart Water Solutions $MgCl_2$ + NaCl (3500 ppm)

The results of total contact angle reduction by using $MgCl_2$ + NaCl smart water (SW) solution are shown in Figure 16. We observed that when $MgCl_2$ is added to NaCl at a concentration ratio of 25%:75%, the reduced contact angle increases from 1.4° to 6.4°, which shows a similar effect with 100% $MgCl_2$. However, the total reduced contact angle decreases when the percentage of $MgCl_2$ increases to 50% and decreases further when the percentage of $MgCl_2$ increases to 75%. Therefore, adding $MgCl_2$ to NaCl could improve the effect of reducing the contact angle of Indiana limestone (ILS) only at a favorable concentrations, which is 25% $MgCl_2$ + 75% NaCl. Moreover, the addition of NaCl into $MgCl_2$ reduces the effectiveness of $MgCl_2$ smart water (SW) solutions due to NaCl is considered to be a non-active ion for low salinity water effect [67–69]. The removal of NaCl also shows an adverse effect in the core-flood experiment in present literature [66]. Besides, no effect of NaCl has also been reported by removing NaCl from seawater by Romanuka and co-workers during their spontaneous imbibition experiments [78].

In conclusion, based on the observation in Section 3.2.3, we believe that the moment we introduce $MgCl_2$ to NaCl (i.e., 50% $MgCl_2$ + 50% NaCl) we have initiated creation of forming ions complexes, which are those ions complexes that make the role of the magnesium (Mg^{2+}) species as wettability alteration agent as ineffective. Additionally, we believe the more we increase the concentration of $MgCl_2$ species concentrations with NaCl (i.e., 75% $MgCl_2$ + 25% NaCl), the more those complexes will form in the presence of NaCl, which makes the role of $MgCl_2$ species more ineffective. It is worth mentioning that further investigations and detailed analysis are needed, which is an anticipated part of our future work. Furthermore, the overall sequence from the lowest reduced contact angle to the highest reduced angle and their total reduced contact angle are given as follows, NaCl (1.4°) < 75% $MgCl_2$ + 25% NaCl (2.4°) < 50% $MgCl_2$ + 50% NaCl (3.2°) < 25% $MgCl_2$ + 75% NaCl (6.4°) ≈ $MgCl_2$ (6.7°).
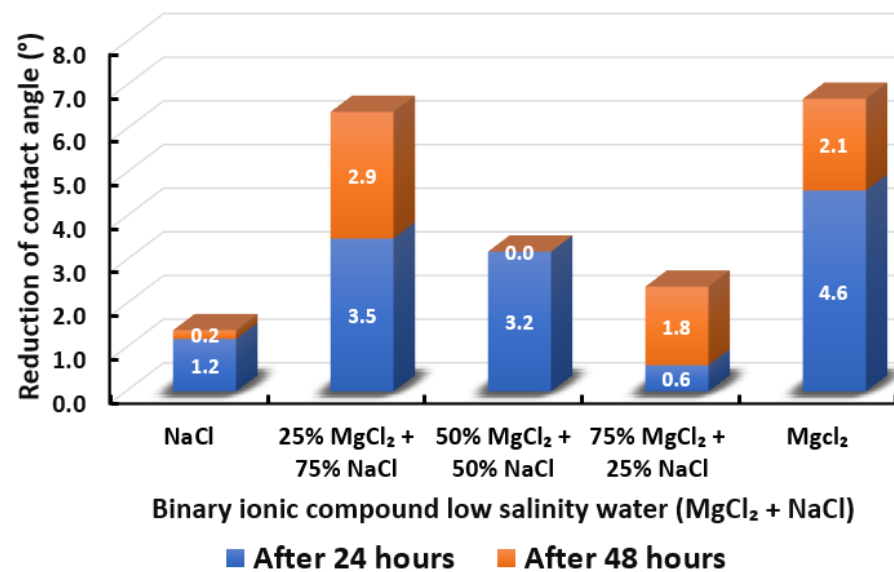
Figure 16. Contact angle reduction results for binary ionic compounds smart water (SW) solutions $MgCl_2$ + NaCl (3500 ppm).

3.2.4. Binary Ionic Compounds Smart Water Solutions $MgCl_2$ + KCl (3500 ppm)

The results of total contact angle reduction by using $MgCl_2$ + KCl smart water (SW) solutions are presented in Figure 17. It is observed that the higher the concentration of $MgCl_2$ (i.e., the lower the concentration of KCl), the higher the reduction of contact angle displayed by Indiana limestone (ILS) up to an equal concentration of both ionic compounds. Further increase of $MgCl_2$ concentration to 75% leads to zero (0) contact angle changes. Consequently, the contact angle changes in the presence of both ionic compounds are maximized at 50% $MgCl_2$ + 50% KCl. Nevertheless, $MgCl_2$ standalone is still able to achieve the highest contact angle reduction. To the best of our knowledge, the effect of KCl to limit $MgCl_2$ efficiency has not been reported in the literature. In conclusion, the overall sequence from the lowest reduced contact angle to the highest reduced angle and their total reduced contact angle are given as follows, 75% $MgCl_2$ + 25% KCl (0°) < KCl (1.3°) < 25% $MgCl_2$ + 75% KCl (2.7°) < 50% $MgCl_2$ + 50% KCl (6.2°) < $MgCl_2$ (6.7°).
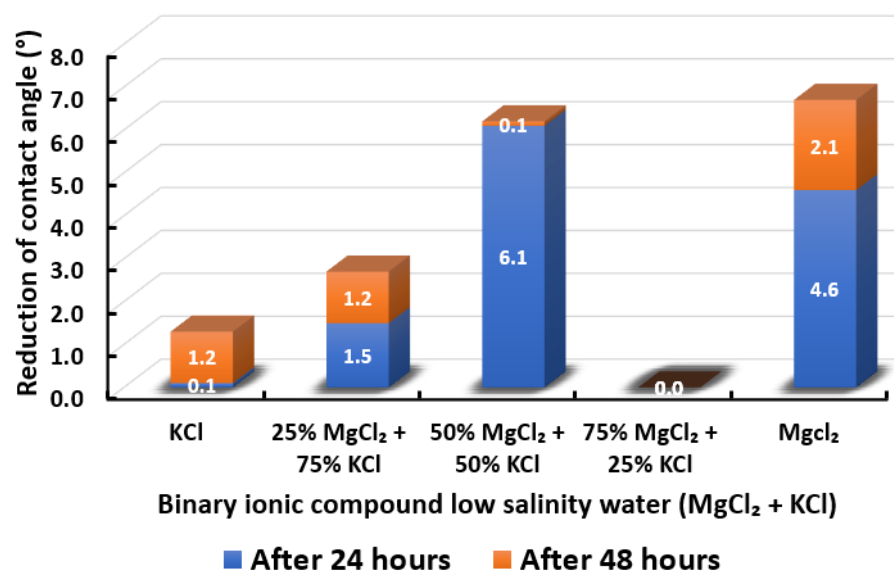
Figure 17. Contact angle reduction results for binary ionic compounds smart water (SW) solutions $MgCl_2$ + KCl (3500 ppm).

3.2.5. Binary Ionic Compounds Smart Water Solutions MgCl$_2$ + CaCl$_2$ (3500 ppm)

Figure 18 illustrates the reduction of the contact angle in the existence of MgCl$_2$ + CaCl$_2$. We observed that when 25% of CaCl$_2$ is replaced by MgCl$_2$, the reduced contact angle drops. However, it gradually increases when the concentration of MgCl$_2$ is increasing and maximizes when the smart water (SW) solution is entirely made up of MgCl$_2$. Consequently, in the presence of MgCl$_2$ + CaCl$_2$ binary smart water (SW) solution, the effect of Mg^{2+} in reducing the contact angle of Indiana limestone (ILS) is more dominant than Ca^{2+}. The effectiveness of Mg^{2+} tends to be reduced in the presence of Ca^{2+}. This observation is similar to the observations made by Al-Attar and co-workers [79]. The highest reduced contact angle that can be achieved by this binary smart water (SW) solution is when smart water (SW) solution is made up of 75% MgCl$_2$ + 25% CaCl$_2$. It has a total of 5.9° change in contact angle but still lower than when MgCl$_2$ is alone, which has 6.7° total change in contact angle. In conclusion, the overall sequence from the lowest reduced contact angle to the highest reduced angle and their total reduced contact angle are given as follows, 25% MgCl$_2$ + 75% CaCl$_2$ (1.6°) < 50% MgCl$_2$ + 50% CaCl$_2$ (2.3°) < CaCl$_2$ (3.5°) < 75% MgCl$_2$ + 25% CaCl$_2$ (5.9°) < MgCl$_2$ (6.7°).
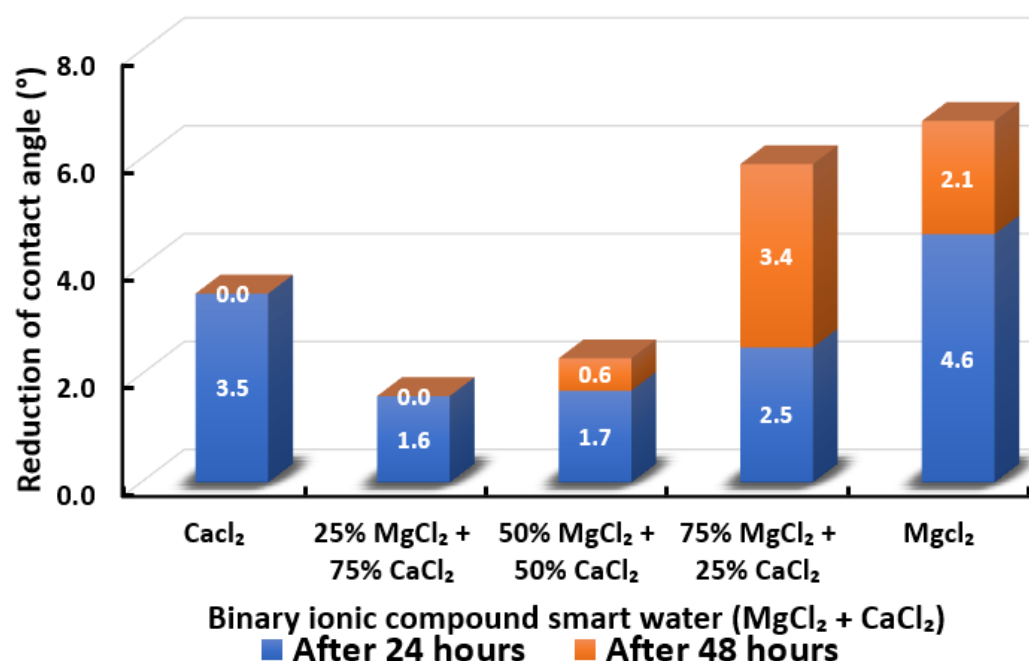
Figure 18. Contact angle reduction results for binary ionic compounds smart water (SW) solutions MgCl$_2$ + CaCl$_2$ (3500 ppm).

3.2.6. Binary Ionic Compounds Smart Water Solutions MgCl$_2$ + Na$_2$SO$_4$ (3500 ppm)

The change in contact angle in the existence of MgCl$_2$ + Na$_2$SO$_4$ is revealed in Figure 19. It is observed that all the combinations could scarcely reduce the contact angle of Indiana limestone (ILS). While MgCl$_2$ and Na$_2$SO$_4$ can reduce the contact angle of Indiana limestone (ILS), the most in the presence of a single ionic compound with low salinity, as shown in Figure 15. However, when MgCl$_2$ and Na$_2$SO$_4$ are mixed as a smart water (SW) solution, almost no reduction of contact angle is attained at any concentration of combination. In conclusion, the overall sequence from the lowest reduced contact angle to the highest reduced angle and their total reduced contact angle are given as follows, 75% MgCl$_2$ + 25% Na$_2$SO$_4$ (0°) ≈ 50% MgCl$_2$ + 50% Na$_2$SO$_4$ (0.3°) ≈ 25% MgCl$_2$ + 75% Na$_2$SO$_4$ (0.6°) < Na$_2$SO$_4$ (4.7°) < MgCl$_2$ (6.7°).
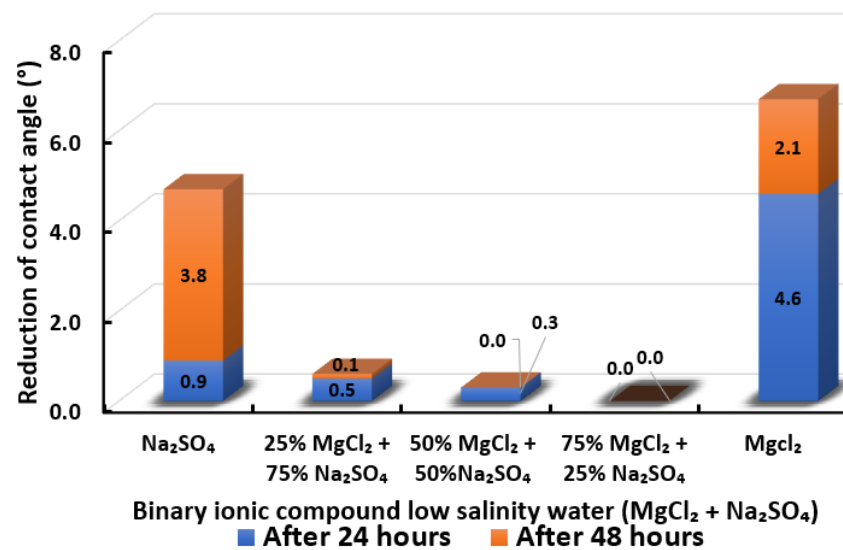
Figure 19. Contact angle reduction results for binary ionic compounds smart water (SW) solutions $MgCl_2$ + Na_2SO_4 (3500 ppm).

3.2.7. Binary Ionic Compounds Smart Water Solutions Na_2SO_4 + NaCl (3500 ppm)

Figure 20 displays the contact angle of Indiana limestone (ILS) modifications in the existence of Na_2SO_4 + NaCl. We observed that Na_2SO_4's or NaCl's standalone presence in smart water (SW) solutions allow more contact angle alterations rather than their combination. Only a minimal contact angle reduction is attained when Na_2SO_4 is mixed with NaCl at every concentration. NaCl is considered as a non-active ion, which may disturb the pathway for SO_4^{2-} to access to the double layer of Indiana limestone (ILS), and consequently reduces surface charge modification for enhancing the oil recovery [67–69]. Moreover, the removal of NaCl also shows an adverse effect in the core-flood experiment in present literature [66]. Besides, no effect of NaCl has been observed by removing NaCl from seawater by Romanuka and co-workers during their spontaneous imbibition experiments [78]. In conclusion, the overall sequence from the lowest reduced contact angle to the highest reduced angle and their total reduced contact angle are given as follows, 75% Na_2SO_4 + 25% NaCl (0.4°) ≈ 25% Na_2SO_4 + 75% NaCl (0.5°) ≈ 50% Na_2SO_4 + 50% NaCl (0.8°) < NaCl (1.4°) < Na_2SO_4 (4.7°).
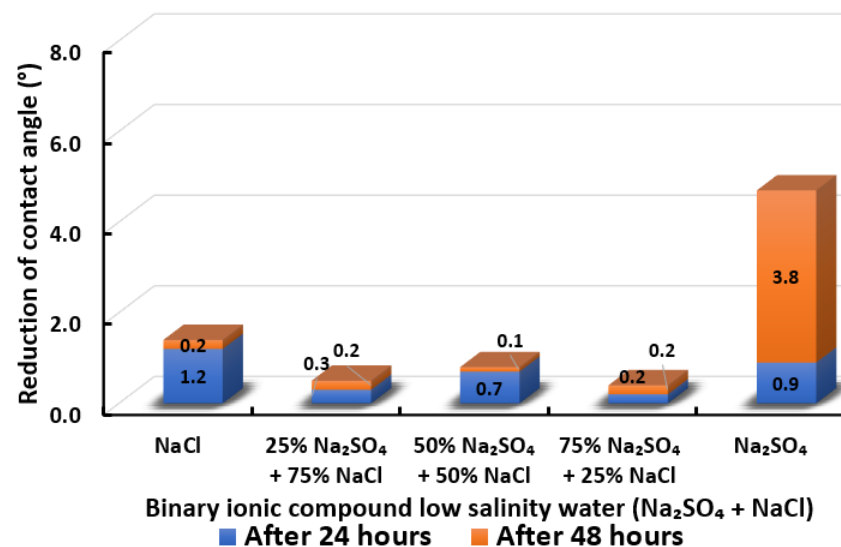
Figure 20. Contact angle reduction results for binary ionic compounds smart water (SW) solutions Na_2SO_4 + NaCl (3500 ppm).

3.2.8. Binary Ionic Compounds Smart Water Solutions Na_2SO_4 + KCl (3500 ppm)

Contact angle reduction for Indiana limestone (ILS) in the presence of Na_2SO_4 mixed with KCl is shown in Figure 21. We observed that the combination of Na_2SO_4 with KCl is not encouraging except for 50% Na_2SO_4 + 50% KCl, which has higher contact angle reduction than (KCl) standalone. In other words, adding 50% of Na_2SO_4 to KCl is able to reduce the total of 3.4° contact angle and enhance the wettability of rock towards more water-wet. On the other hand, Na_2SO_4 standalone yields the highest contact angle reduction. It is consequently concluded that KCl might also act as a barrier for SO_4^{2-} in changing the surface charge of rock and thus minimize the contact angle shift. In conclusion, the overall sequence from the lowest reduced contact angle to the highest reduced angle and their total reduced contact angle are given as follows, 75% Na_2SO_4 + 25% KCl (0°) < 25% Na_2SO_4 + 75% KCl (0.6°) < KCl (1.3°) < 50% Na_2SO_4 + 50% KCl (3.4°) < Na_2SO_4 (4.7°).
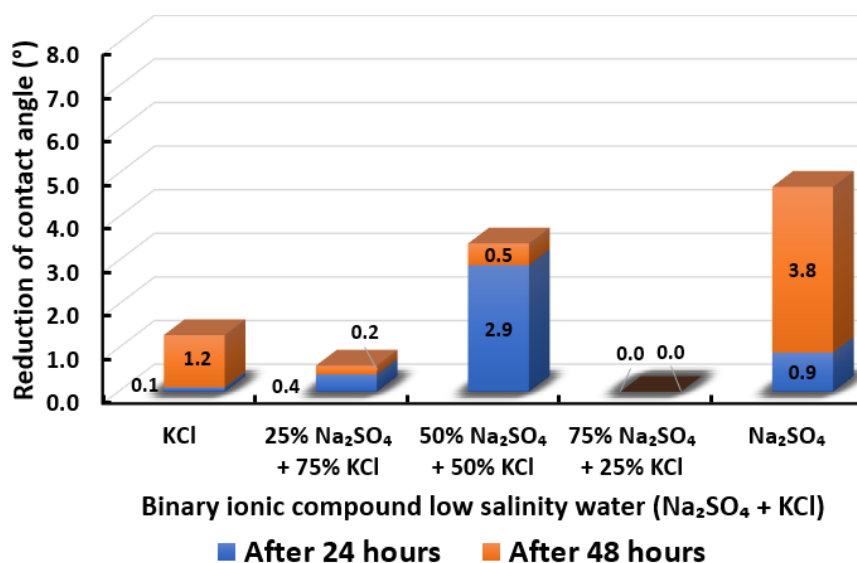
Figure 21. Contact angle reduction results for binary ionic compounds smart water (SW) solutions Na_2SO_4 + KCl (3500 ppm).

3.2.9. Binary Ionic Compounds Smart Water Solutions Na_2SO_4 + $CaCl_2$ (3500 ppm)

Figure 22 illustrates contact angle reduction for the binary smart water (SW) solution of Na_2SO_4 + $CaCl_2$. There is no particular trend observed for the effect of Na_2SO_4 and $CaCl_2$ concentration in this binary smart water (SW) solution. Equal concentrations of Na_2SO_4 + $CaCl_2$ result in negligible contact angle changes and no significant contact angle reduction differences when replacing 25% of $CaCl_2$ with Na_2SO_4. Combining Na_2SO_4 with $CaCl_2$ is anticipated to increase oil recovery further, as observed in the work of Zhang and Austad [74,75]. Interestingly, only 75% Na_2SO_4 + 25% $CaCl_2$ can induce higher total contact angle reduction in this experimental work. This combination manages to reduce contact angle for a total of 8.2° compared to the total contact angle reduction exhibited by 100% Na_2SO_4 and 100% $CaCl_2$ which are 4.7° and 3.5°, respectively. Consequently, the interaction of Na_2SO_4 with $CaCl_2$ is effective in reducing contact angle to more hydrophilic (water-wet) only when both are mixed with in the right combined concentration. Under an unfavorable percentage combination of Na_2SO_4 with $CaCl_2$, calcium sulphate formation might occur. This would decrease the concentration of active ions block porous media of Indiana limestone (ILS) [80–82] and affect the efficiency of Na_2SO_4 + $CaCl_2$ smart water (SW) solution in altering the wettability of Indiana limestone (ILS). In conclusion, the overall sequence from the lowest reduced contact angle to the highest reduced angle and their total reduced contact angle are given as follows, 50% Na_2SO_4 + 50% $CaCl_2$ (0.1°) < $CaCl_2$ (3.5°) ≈ 25% Na_2SO_4 + 75% $CaCl_2$ (3.6°) < Na_2SO_4 (4.7°) < 75% Na_2SO_4 + 25% $CaCl_2$ (8.2°).
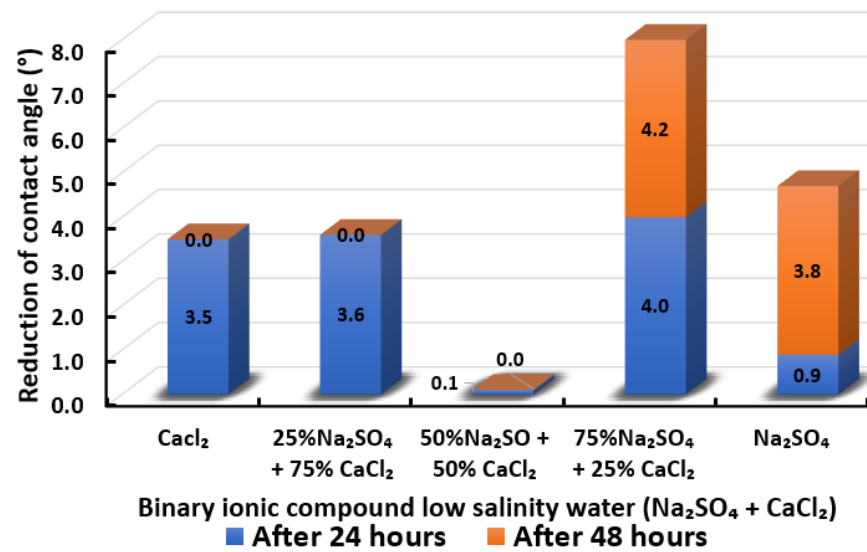
Figure 22. Contact angle reduction results for binary ionic compounds smart water (SW) solutions Na_2SO_4 + $CaCl_2$ (3500 ppm).

3.2.10. Selection of Smart Water Solutions (1750 ppm and 3500 ppm)

The highest and lowest contact angle change for seawater dilution, and the highest (e.g., the best four) contact angle change for smart water (SW) solutions are selected for further study on the drivers of ionically modified brine solutions in ILS carbonate rocks. Seawater diluted to 20-times 1750 ppm (i.e., highest change in contact angle) and seawater (35,000 ppm) (i.e., lowest change in contact angle) were selected from dilution category while 75% Na_2SO_4 + 25% $CaCl_2$ (3500 ppm), $MgCl_2$ (3500 ppm), 25% $MgCl_2$ + 75% NaCl (3500 ppm), and 50% $MgCl_2$ + 50% KCl (3500 ppm) were selected from smart water (SW) category. The contact angle results for these six selected solutions (i.e., smart water and seawater) are shown in Figure 23. The repeated dynamic contact angle modifications for seawater, diluted seawater, and smart water solutions are presented in Figures A1–A25 (see Appendix A).
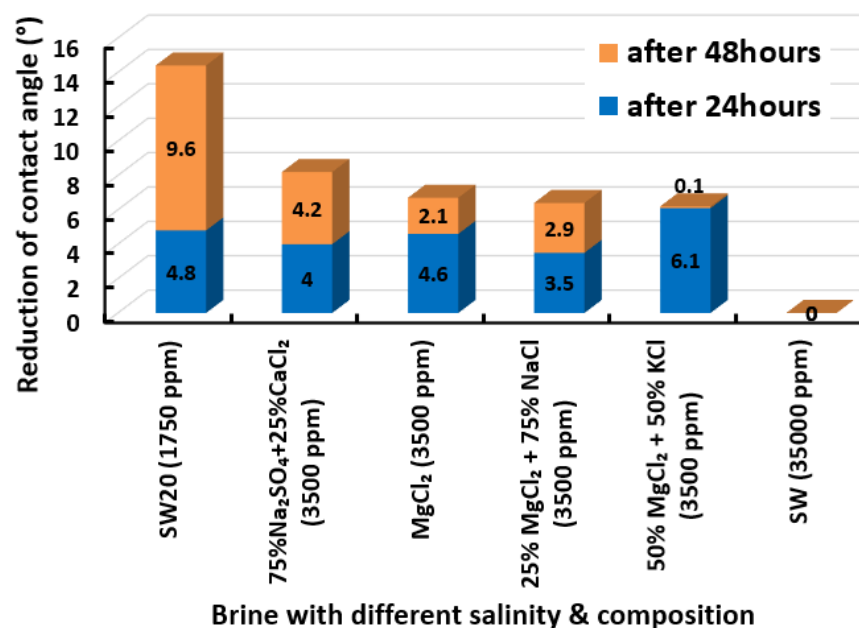
Figure 23. Contact angle reduction results; six selected smart water (SW) solutions.

3.3. Zeta Potential Test (ZPT)

Zeta potential (ZP) measurement is done to study and observe the impact of our proposed smart water (i.e., ionically modified brine) solutions on surface charge modification of carbonate rocks. Figures 24 and 25 show the effect of seawater, diluted seawater, and smart water (SW) solutions on surface charge modification of Indiana limestone (ILS) carbonate rocks. Figure 25 shows the effect of brine solutions containing divalent ions $(MgCl_2)$ on the behavior of surface charge alteration, and thus the surface potential modifications; the six brine solutions selected for the zeta potential (ZP) measurement are seawater (35,000 ppm), 20-times diluted seawater (1750 ppm), 75% Na_2SO_4 + 25% $CaCl_2$ (3500 ppm), $MgCl_2$ (3500 ppm), 25% $MgCl_2$ + 75% NaCl (3500 ppm), and 50% $MgCl_2$ + 50% KCl (3500 ppm). The results in Figure 4.45 show that diluted seawater and smart water (SW) solutions can alter the surface charge and consequently has a significant impact on Indiana limestone (ILS) surface charge modifications. It should be noted that all ZP measurements for the six selected brine solutions were measured at the pH value range between 6.45 and 7.80, as shown in Table 8.

Table 8. Results of pH value for the six selected brine solutions at ambient conditions.

Components	pH Value	Temperature (°C)
Seawater (35,000 ppm)	7.80	23.7
20 times diluted seawater (1750 ppm)	7.70	23.9
Na_2SO_4 + $CaCl_2$ (3500 ppm)	6.69	24.0
$MgCl_2$ (3500 ppm)	6.83	24.4
25%$MgCl_2$ + 75%NaCl (3500 ppm)	6.45	24.3
50%$MgCl_2$ + 50%KCl (3500 ppm)	6.70	23.8
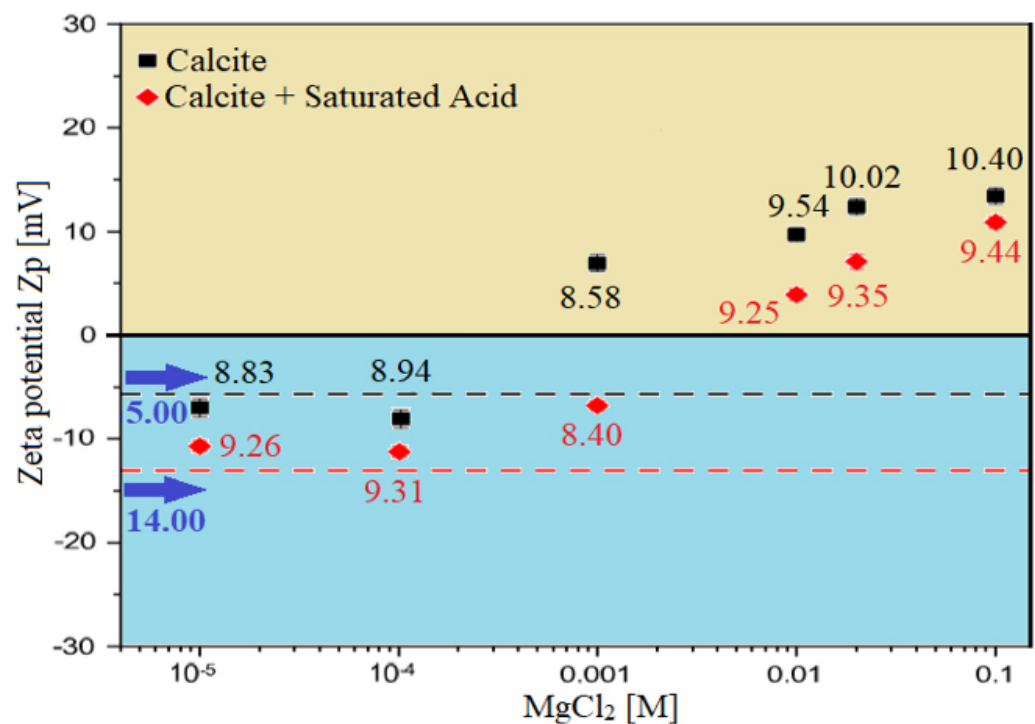
Figure 24. Zeta Potential (ZP) of calcite carbonate rocks/brine interface; It shows the effect of brine solutions containing divalent ions $(MgCl_2)$ on the behaviour of surface charge alteration on calcite rock surfaces.
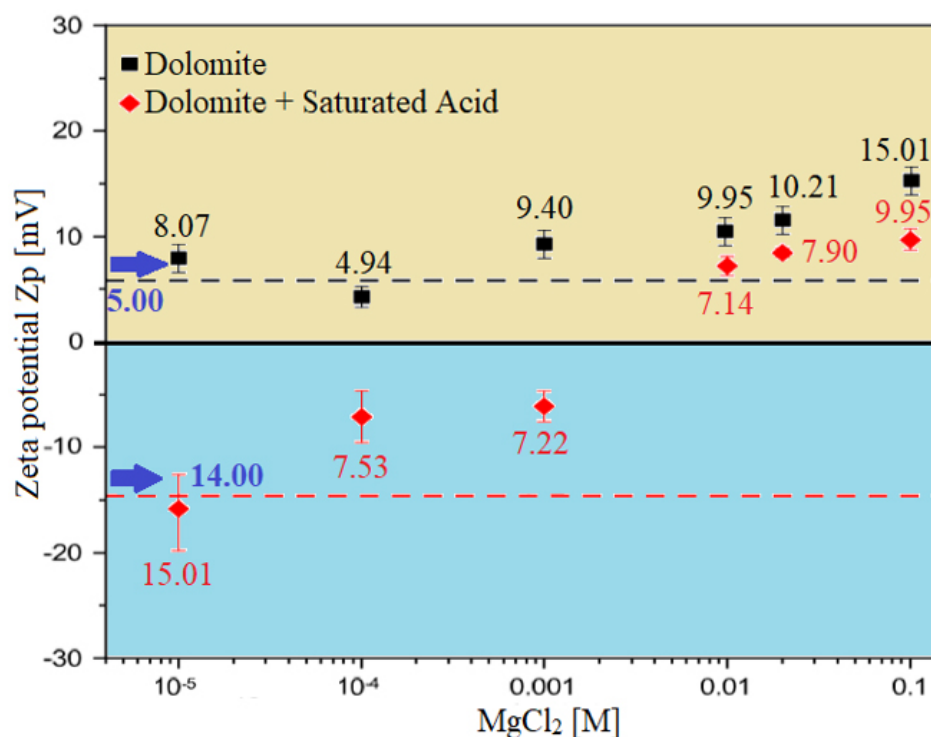
Figure 25. Zeta Potential (ZP) of dolomite carbonate rocks/brine interface; It shows the effect of brine solutions containing divalent ions (MgCl$_2$) on the behaviour of surface charge alteration on dolomite rock surfaces.

3.3.1. Zeta Potential at Brine–Rock Interface

The blue-colored bar columns in Figure 26 represent the surface potential (i.e., electrokinetic potential or zeta potential) at the brine and Indiana limestone (ILS) interface for seawater, diluted seawater, and smart water (SW) solutions at elevated temperature of 80 °C. For salinity dilution, the zeta potential of high salinity seawater (35,000 ppm) is increased from +6.94 mV to +14.52 mV when it is diluted to 20-times (1750 ppm). This increasing trend is similar to the surface complexation modeling (SCM) results of Hassan et al. [29,31]. This phenomenon might be attributed to the surface complex distributions at Indiana limestone surface and brines interface, and consequently the rock surface becomes more positive. This phenomenon might be attributed to the surface complexes distributions at the Indiana limestone's surface and brines interface. Moreover, the brine and ILS interface are positively charged, as shown both in Figures 25 and 26. This is due to the fact that the ILS used in this experimental work is predominantly made from calcite (i.e., 92.03 % of CaCO$_3$), which is originally positively charged, as shown in X-ray diffraction (XRD) analysis results in Figure 11. A contrary trend is observed for (75% Na$_2$SO$_4$ + 25% CaCl$_2$). This might occur due to the adsorption of SO_4^{2-} on the Indiana limestone surface [83]. Since 75% is made up of Na$_2$SO$_4$, more SO_4^{2-} are being attracted to positively charge Indiana limestone and make the surface become negatively charged leading the zeta potential at the Indiana limestone and brine interface to be reduced to −5.01 mV. Sari and co-workers [84] also observed that SO_4^{2-} has a stronger affinity towards the rock surface than a carboxylic group of crude oil and change rock charge from positive to negative. This is consistent with existing data, which concluded that increasing concentration of SO_4^{2-} could cause a more negative surface potential or reduce positive surface potential [85–87]. Additionally, Alotaibi and co-authors [88,89] have also attained negative zeta potential for ILS particles in Na$_2$SO$_4$ brine.
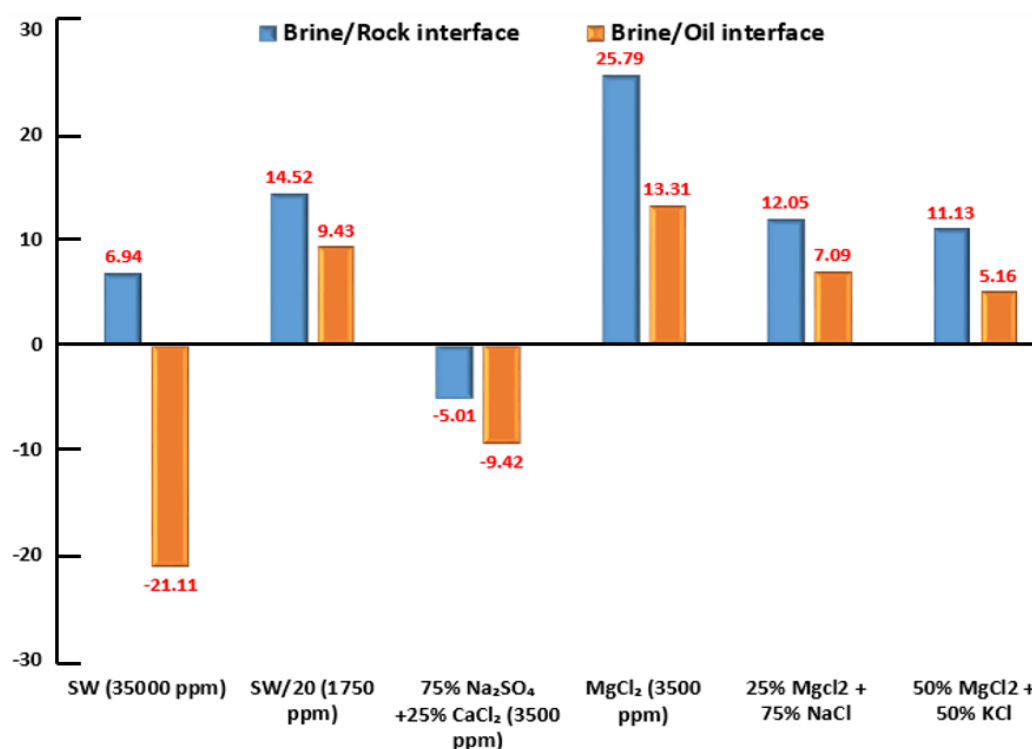
Figure 26. Zeta Potential (ZP) of brine/rock interface and brine/crude oil interface in different brine solutions at reservoir temperature of (80°C); SW (35000 ppm) and SW/20 denote seawater and 20-times diluted seawater respectively; all six brine solutions have a pH-value range between (6.45) and (7.80), as shown in Table 8.

3.3.2. Zeta Potential at Crude Oil-Brine Interface

The orange-colored bar columns in Figure 26 represent the surface potential (i.e., electro-kinetic potential or zeta-potential) at the brine and crude oil interface for seawater, diluted seawater, and smart water (SW) solutions at an elevated temperature of 80 °C. Besides, each brine solution impacts the surface potential (i.e., electro-kinetic potential) between the crude oil and brine solution interface. In general, the crude oil/brines interface has a negative zeta potential due to a negatively charged polar group (carboxylic acid group) in the crude oil [88,89]. However, the surface potential or zeta potential for the brine/crude oil could be positive as investigated by Jackson and co-authors [90]. Sari and co-workers [84] have also reported a positive zeta potential for the brine/crude oil interface. Consequently, the crude oil/brine interface's surface potential is somehow related to the interaction between crude oil and the ion's presence in the brine solution.

3.3.3. Interaction between Two Interfaces

Figure 26 displays both blue and orange-colored bar columns to illustrate the interactions between crude oil–brine and brine–rock interfaces. We observed similar positive signs of surface charges at the crude oil–brine and brine–rock interfaces in the presence of diluted seawater (1750 ppm), $MgCl_2$ (3500 ppm), 50% 25% $MgCl_2$ + 75% NaCl (3500 ppm), and 50% $MgCl_2$ + 50% KCl (3500 ppm). We observed similar negative signs for the surface charges at the crude oil-brine and brine-rock interfaces by 75% Na_2SO_4 + 25% $CaCl_2$ (3500 ppm). Both similar positive and negative signs of surface charges at crude oil–brine and brine–rock interfaces indicate that both interfaces repel each other representing repulsive forces between crude oil–brine and brine–rock interfaces. Therefore, the water film in between two interfaces remains stable [30,31]. In other words, these brine solutions as mentioned above, can alter the rock wettability of ILS towards the more water-wet state. These results are in line with the contact angle measurements results as well as the SCM results proposed by Hassan et al. [30,31]. On the other hand, we observed different signs of surface charges

at brine/rock (i.e., positive sign) and brine/crude oil (i.e., negative sign) interfaces in the presence of seawater (35,000 ppm), which indicate that both interfaces attract each other. Therefore, the water film in between two interfaces collapses. In other words, for the approach adopted, it appears that a high salinity seawater (35,000 ppm) solution is not able to change the rock wettability of ILS towards a more water-wet state. These results are also in agreement with the contact angle measurements results as well as the SCM results by Hassan et al. [30,31].

3.4. Aqueous Stability Test (AST)

As previously discussed in Section 2.2.4, the primary objective of the aqueous stability test (*AST*) is to determine the brine solution that can form a stable and transparent (clear) FW at a temperature of 80 °C with the selected surfactant. If the FW forms precipitation, it may create a non-uniform distribution or clog the reservoir rocks' pore throats, which leads to an ineffective oil recovery or reservoir damage [91]. This consents to the choice of the best surfactant aqueous solution (FW) for the other tests, viz., foamability and foam stability test. To conclude, the result of these six selected smart water and seawater solutions (e.g., $MgCl_2$ and NaCl) when we mixed with different type of surfactant (e.g., CTAB and AOS) were clear (i.e., no precipitation was observed at 0, 6, 12, 24, 48, 72 h at a temperature of 80 °C).

3.5. Foamability and Foam Stability Test (FT and FST)

Since our goal is to design smart water (SW) solutions that have a dual effect on wettability alteration and foam stability, the best six smart water (SW) solutions that resulted in the highest wettability modifications were selected in this part of the screening process. During foam formation, foamability, and foam stability were studied for each selected surfactant with different concentrations by introducing nitrogen (N_2) and carbon dioxide (CO_2) gas volumes of 25 and 50 cc (cubic centimeter) for 20 s. This corresponds to the average volumetric rates of 4.5 and 9.0 L/h (litter per hour), respectively. Figures 27–30 summarize the foamability tests for all surfactant aqueous solutions (SAS) investigated. Figure 27 shows the initial foam height of the CTAB (cetyltrimethylammonium bromide) surfactant solutions as a function of gas type (N_2 and CO_2) for different type of brine solutions (i.e., the six selected brine solutions) at fixed surfactant concentrations (1000 ppm). The figure displays a two times higher foam height when gas injection was doubled from 4.5 to 9 (L/h) for both nitrogen (N_2) and carbon dioxide (CO_2) gas injection. However, the general trend is that the nitrogen (N_2) gas injection showed a higher foam height than the carbon dioxide gas injection. The same trend is observed in the case of DTAB, AOS, and alpha-foamer surfactants solutions, as shown in Figures 28–30, respectively.

In summary, all surfactants (i.e., CTAB, DTAB, AOS, and alpha-foamer) solutions can be characterized with good foamability during foam column formation for both nitrogen (N_2) and carbon dioxide (CO_2) gas injection.

Moreover, the effect of water chemistry (i.e., change composition and salinity) on foam stability was tested by comparing the R5 results of a selected type of surfactant (e.g., CTAB, AOS, and alpha-foamer) solutions at different brine solution with different compositions and salinity level (e.g., seawater, 20-times diluted seawater, and our designed smart water solutions). Figure 31 summarizes the foam stability tests results. Figure 31 displays the (R5) values as a function of surfactant concentrations for several selected surfactant aqueous solutions (SAS). The results show that the smart water solution ($MgCl_2$) (3500 ppm) has the highest (R5) stability percentage (90%) compared to seawater (35,000 ppm) R 5 = 0%), which shows the lowest foam stability. Finally one should note that based on the surfactant concentration analysis in Figure 31, a surfactant concentration of 1000 ppm was used for further studies.
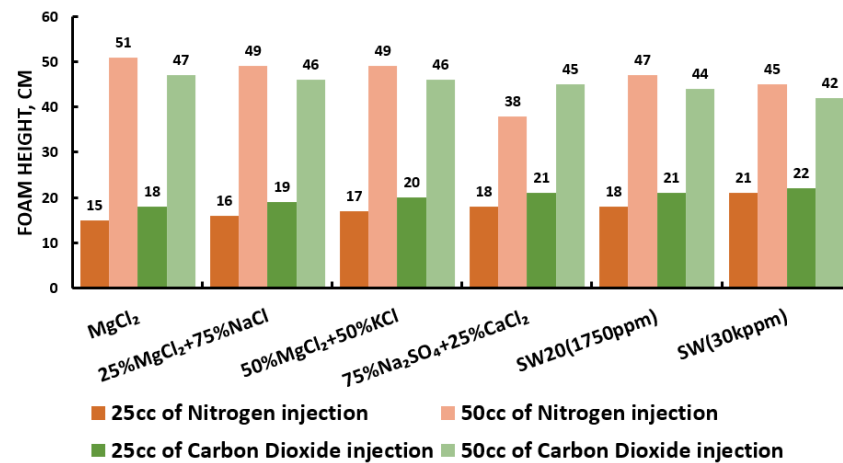
Figure 27. Surfactants screening: foamability test—CTAB at 25 °C.
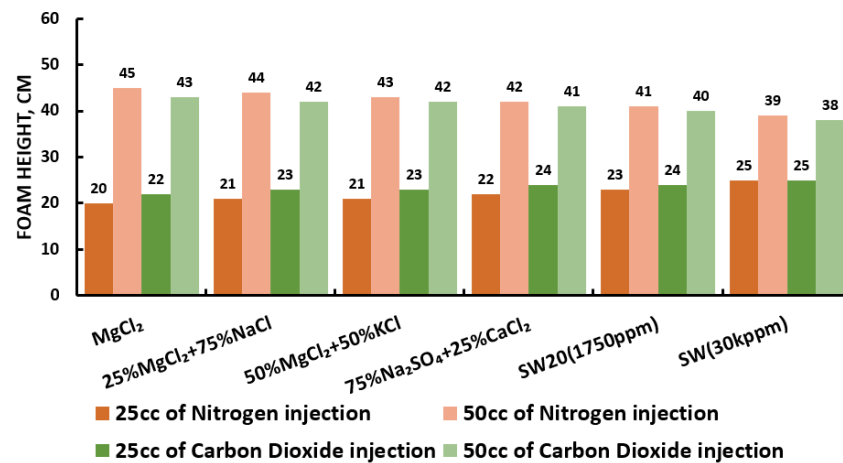
Figure 28. Surfactants screening: formability test—DTAB 25 °C.
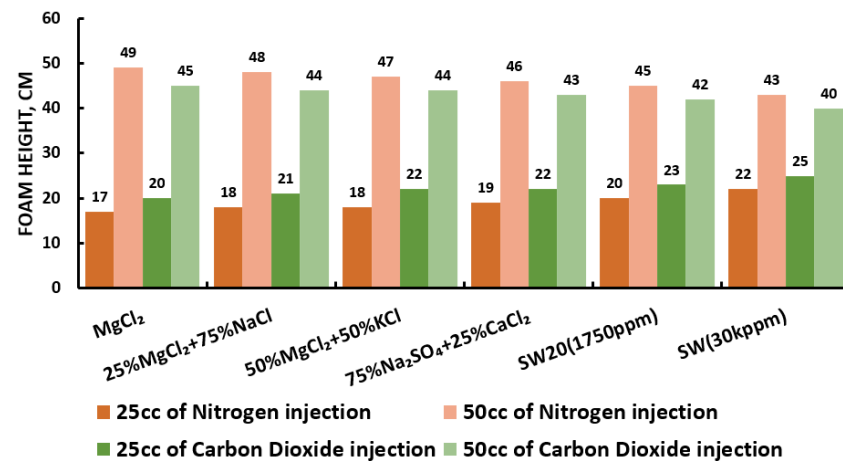
Figure 29. Surfactants screening: formability test—AOS 25 °C.

Finally, since foam is thermodynamically unstable, it is important to predict and investigate the foam stability [92–94]. A significant concern when using foam for mobility control is its stability in the presence of oil. Foam stability of different surfactant aqueous solutions (SAS) was tested in the presence of oils (e.g., Type A), and the results attained were compared with those achieved previously as shown in Figure 31. The results of Figure 32 reveal that in the presence of oil and as expected, all SAS (i.e., surfactant aqueous

solutions) show lesser foam stability compared with those attained previously (i.e., the R5 stability percentage decreases approximately 10%) [42].
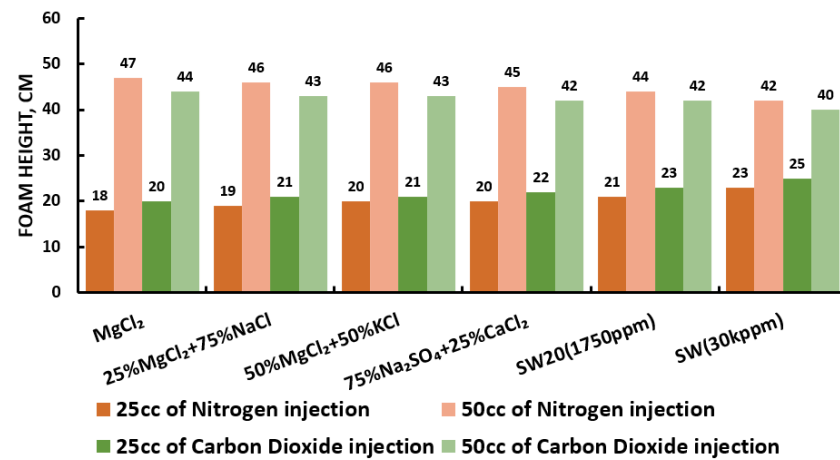
Figure 30. Surfactants screening: formability test—alpha-foamer 25 °C.
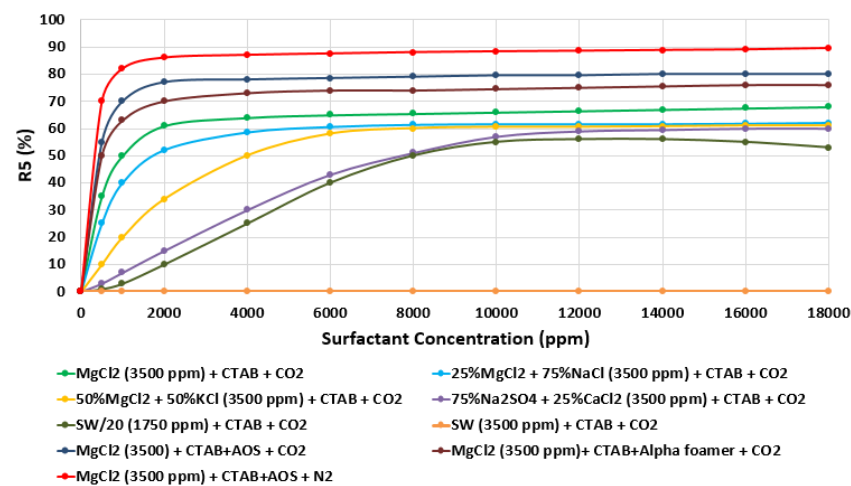
Figure 31. Variation of R5 (in percentage (%)) as a function of surfactant concentration (ppm) of different surfactant (e.g., CTAB and AOS) and various brine solutions (e.g., MgCl$_2$ and seawater) at 25 °C.
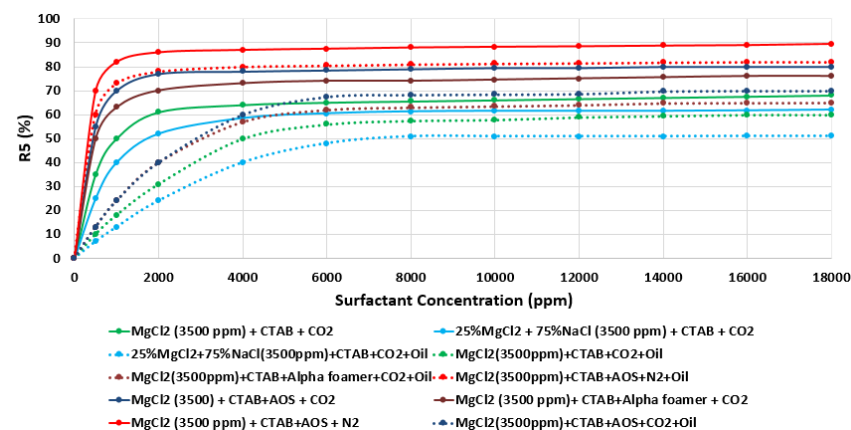
Figure 32. Variation of R5 (%) as function of surfactant concentration (ppm) of different tested surfactant (e.g., CTAB, AOS, and alpha-foamer) at various brine solutions in the presence of crude oil at (25 °C).

3.6. Core-Flooding Test

Based on the screening process presented earlier, numerous core-flooding tests (runs) were conducted to investigate the efficiency of successful smart water (SW) solutions and surfactant aqueous solutions (SAS) candidates to generate foam in porous media in the presence of crude oil (Type A and Type B). Three SWAF injection scenarios, viz., $MgCl_2$, 25% $MgCl_2 + 75\% NaCl$, and SAS with four sequence-scenarios of SAS alternating gas (SAG) and different slug sizes at two types of crude oil (Type A and Type B) were conducted to investigate the optimum slug sequence-scenario that leads to high recovery factor. Figure 12 shows the injection scenario of $MgCl_2$ smart water solution (3500 ppm). Based on the core flooding test results, the recovery factor of SWAF process is up to 42% incremental recovery of oil initial in core or OIIC (i.e., 92% of the cumulative OIIC), which represents an optimistic scenario (i.e., in the case of $MgCl_2$ based smart water solution with CTAB at 1000 ppm), as shown in Figures 33 and 34. In the Figures 33 and 34, the primary injection scheme represents the formation water (FW) injection. The secondary injection scheme represents the injection of the ionically modified brine (i.e., low salinity or smart water solution). The EOR or tertiary injection mode represents the SAG (i.e., SAS alternating gas) injection, which consists of SAS, gas, SAS, and gas injection.

It is worth mentioning that we conducted the foamability (FT) and foam stability tests (FST) using state-of-the-art R5 parameter tests at 25° room temperature and an atmospheric pressure of 1 (atm) to screen the stability of our designed SAS formulations. However, based on the result of the R5 (%) parameter, we got a stable foam and in the case of 100% $MgCl_2$ and $MgCl_2$ combined with NaCl. Then, we proceeded with the core flood at a replicated reservoir temperature of 80°, confining pressure of 2700 psi, and a back pressure of 2300 psi. We obtained high oil recovery and we observed the foam propagation (in the produced fluid) continue pouring out of the outlet of the graduated tube from the fraction collector. This indicated that the foam is metastable (see Figure 35) i.e., the foam retained its stability at the replicated reservoir conditions and did not decay. Additionally, we know the fact that the foamability and foam stability tests were conducted at laboratory scale at ambient conditions, and performing the tests at reservoir scale conditions could have proved to be a different game altogether. Even so, for the proof of concept of the SWAF technique at laboratory scale, we performed the tests and obtained very promising results. Additional details on the subsequent studies shall be part of our forthcoming works.

In addition, it is important to note that in Figure 33, which illustrates the SWAF injection scenario to study the effect of crude oil Type A and Type B, there were no significant contrast in incremental recovery factors for primary, secondary and ternary (EOR) modes. This no significant contrast in results of incremental oil recovery factors can be explained on the basis of the following;

- Core sample properties: In all injection scenarios we have used Indiana limestone (ILS) core samples with similar petrophysical properties (known as sister core samples). Our ILS cores samples are in the same range of permeability (i.e., 50–100 mD) and porosity (14–19%), as shown in Tables 6 and 7.
- Crude oil properties: There were no significant contrasts in the two crude oil (Type A and Type B) properties in terms of API degrees of 28.42 and 30.26, respectively, TAN of 1.17 and 0.81 mgKOH/g, respectively, and TBN of 0.23 and 0.59 mgKOH/g, respectively, as specified in Table 2.
- Moreover, in the literature [95] where different crude oils with acid and base numbers (TAN and TBN) were studied, it became apparent that only those crude oils having significant contrast (e.g., 4-times greater difference [95]) in TAN will trigger a more pronounced difference in oil recoveries.

Finally, the optimum SWAF injection scenario (i.e., $MgCl_2$ based smart water solution with CTAB at 1000 ppm) is optimized by studying the effect of the slug size of the smart water (SW) injection. It was observed that changing the slug size of the SW injection scenario from 5 PVs to 2 PVs leads to more OIIC recovery as shown in Figure 36. In addition, Hassan et al. [32] conducted exergy (i.e., a useful amount of net energy) return on

exergy invested analysis, which showed that the main contributor for the exergy investment is the cost of fluid circulation. The fluid circulation costs accounted for 80% of exergy invested, while, the chief contributor for the exergy gained is the produced oil/recovered oil. Thus, when the exergy invested to exergy return ratio is <1, the scheme is profitable with low environmental impact due to low CO_2 footprint. on the other hand, when exergy investment exceeds the exergy invested, making the ratio >1, it means that the production must be stopped due to the high CO_2 footprint [32]. Moreover, during the evaluation of SWAF slug sizes in their investigational study, it was realized that the 5 PVs scenario involved higher exergy invested to exergy return due to higher fluid circulation costs with lower oil recovery. Whereas, when 2 PVs slug size was used instead, there were lower fluid circulation costs involved and hence more returns through increased recovery. Therefore, by changing the slug size of the SWAF injection scenario from 5 PVs to 2 PVs, more oil recovery was observed, which is highly lucrative. Additionally, reducing the slug size from 5 PVs to 2 PVs reduced the fluid circulation costs, which limits the CO_2 footprint. Hence, the proposed SWAF process, when under optimum controlled conditions, can be an economically attractive EOR technique while also being environmentally suitable [32].
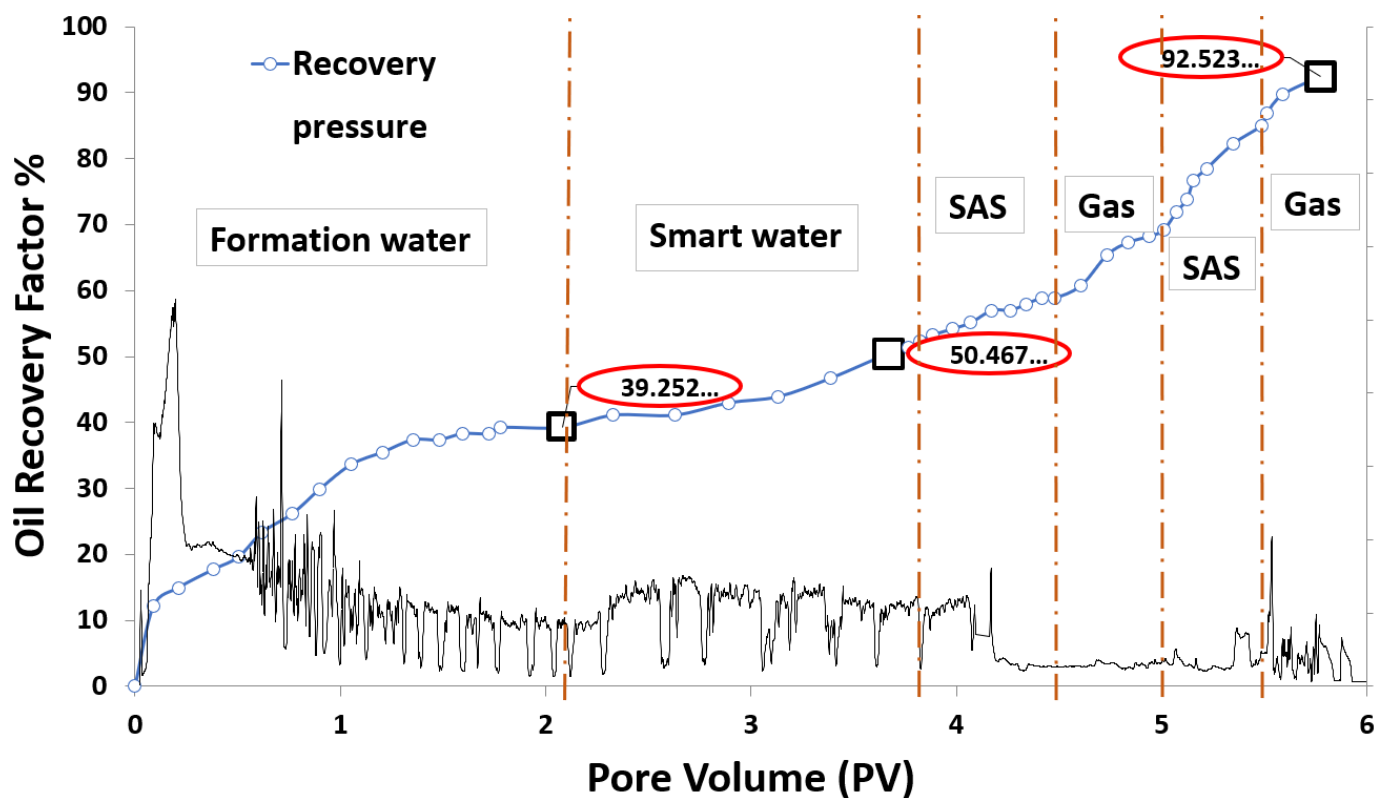
Figure 33. Smart water-assisted foam (SWAF) injection process for the best case scenario (i.e., $MgCl_2$), The method works as an improved/enhanced (IOR/EOR) recovery method for the ionically-modified brine, which goes up to 39% RF for the primary stage (i.e., formation water), 11% RF (i.e., 50% cumulative OIIC) for the secondary stage (i.e., smart water injection), and 92% cumulative OIIC for the tertiary stage (SAG injection i.e., SAS, gas, SAS, and gas).
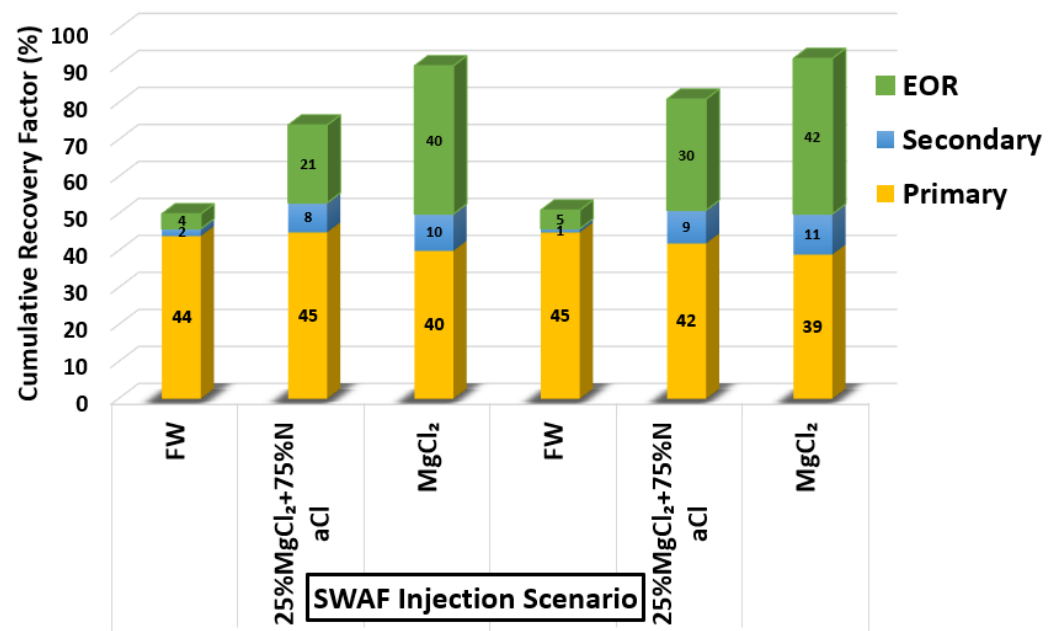
Figure 34. Smart water-assisted foam (SWAF) injection scenarios; the effect of crude oil type (Type A and Type B) with different smart water (SW) solutions (i.e., 3500 ppm) and at surfactant concentration of 1000 (ppm). For the best-case scenario (i.e., $MgCl_2$), the method works as an improved/enhanced (IOR/EOR) recovery method for the ionically modified brine, which goes up to 39% RF for the primary stage (i.e., formation water), 11% RF (i.e., 50% cumulative OIIC) for the secondary stage (i.e., smart water injection), and 92% cumulative OIIC for the tertiary stage (SAG injection i.e., SAS, gas, SAS, and gas).
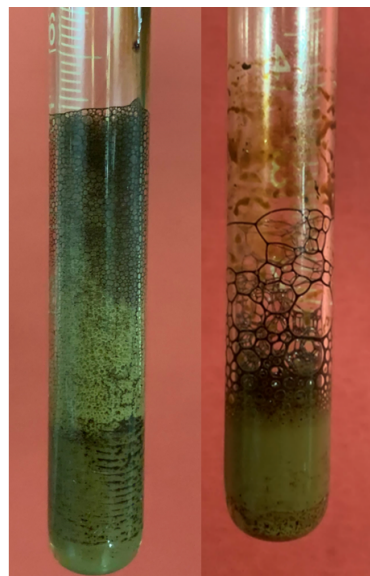
Figure 35. During core flooding experiments, we obtained high oil recovery (up to 92% cumulative OIIC, as shown in Figures 33 and 34, and we observed the foam propagation (in the produced fluid) continue pouring out of the outlet of the graduated tube from the Fraction Collector. This indicated that the foam is metastable i.e., the foam retained its stability at the replicated reservoir conditions and did not decay confirming the results of Figures 31 and 32 the fraction collector. The produced fluid from the Indiana limestone (ILS) core samples was collected in graduated tubes.
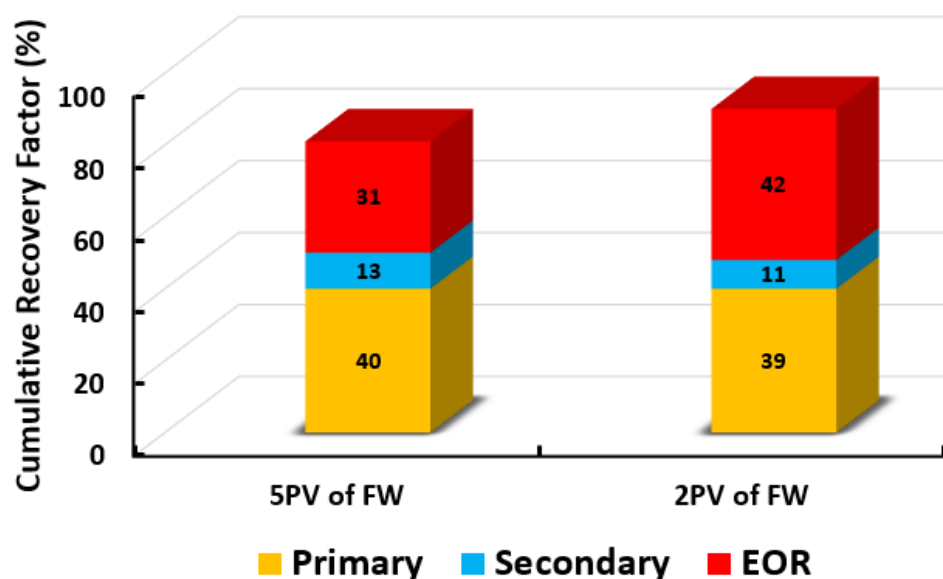
Figure 36. The effect of slug size of smart water injection ($MgCl_2$ + oil Type A); The case of SWAF injection scenario with 2 PVs leads to more EOR recovery compare 5 PVs. Besides, it has less fluid circulation costs and thus has a lower CO_2 footprint.

4. Summary and Conclusions

This contribution aimed at proposing a new hybrid EOR technique by combining smart water (SW) injection and foam flooding in carbonate reservoirs, known as smart water-assisted foam (SWAF) flooding or SWAF process. The main function of the SWAF process is to displace crude oil to the production wells by the injection of smart water (SW) followed by an alternating injection of a surfactant aqueous solution (SAS) and gas, termed SAG. Usually, carbonate reservoirs, which are mixed to oil-wet in nature, suffer from low productivity during secondary and tertiary recovery modes due to several factors. Among those factors are, (i) water injection is not effective due to strong adsorption of the crude oil on carbonate rock surface (i.e., water film collapses), and (ii) the decay of the foam when it gets in contact with crude oil during foam flooding (i.e., foam lamella collapses) [13,19,27,28]. To overcome these problems, our smart water is designed in such a way that it can alter the carbonate rock wettability and at the same time can improve the foam film stability by minimizing the shielding effect of the electrical double layer or EDL (i.e., the characteristic of dual improvement effect resulting in compounded oil displacement) [30,31]. In the SWAF process, our designed smart water (i.e., ionically modified brine) is characterized by a dual-improvement effect, which is a novel concept introduced through this contribution. Firstly, the SW injection modifies the rock wettability from mixed to oil-wet towards a more water-wet state (i.e., enhance the water film stability). Secondly, the smart water also stabilizes the foam film lamellae leading to improved oil displacement. Furthermore, the SWAF technology possesses the synergy effect of combining smart water with foam flooding (SAS alternating gas i.e., SAG), which produces further wettability alteration and IFT reduction that creates conditions for more favorable relative permeability behavior. The interfacial tension (IFT) reduction occurs by adding surfactants to the smart water solution (i.e., SAS formulations). During the foam flooding stage, it is favorable in increasing ultimate oil recovery [20,42]. At the same time, to the best of our knowledge, there have not been any experimental nor investigational works of literature discussing the dual-improvement effect of wettability alteration and foam stability using smart water (SW) in carbonates. Additionally, no publications were available regarding the synergy effects of combining smart water with foam flooding i.e., SWAF process in carbonate reservoirs.

Furthermore, a series of laboratory experiments (i.e., investigation techniques) were conducted to investigate the water film (i.e., wettability measurements) and foam lamellae

(foamability and foam stability tests) stability for our SWAF crude oil/brine/rock interactions (COBR system). A first screening process was used to narrow down candidate designed smart water (i.e., ionically modified low salinity brine) solutions with the contact angle tests using calcite plate (Indiana limestone or ILS) as the first filter. Then, optimum smart water (SW) candidates were mixed with different types of (i.e., cationic and anionic) surfactants to generate optimum surfactant aqueous solution (SAS). After that a second screening process was used to narrow down candidates SAS with different types of gases (CO_2 and N_2) by conducting aqueous stability tests (*AST*), foamability (IFT), and foam stability tests (FST). Successful combination of SAS and gas candidates were confirmed by the core flooding test (CFT). The main findings of the laboratory work are as follows;

- Our designed smart water (SW) has the characteristic of dual improvement effect resulting in compounded oil displacement. Both the fluid–rock (i.e., brine–rock) and fluid–fluid (i.e., brine/oil) interactions are affected by the designed SW solutions.
- The effect of the potential determining ions or PDIs (i.e., Mg^{2+}) presence on surface charge alteration is one of the fundamental requirements for the performance of our designed smart water solution to alter the carbonate rock wettability toward more water-wet condition [30,31].
- To identify the optimum smart water solutions, wettability measurements revealed that 100% $MgCl_2$ (i.e., 3500 ppm) (PDIs) and 20-times diluted seawater (1750 ppm) can alter the surface charge and consequently has a significant impact on Indiana limestone (ILS) surface charge modifications, as shown in Figure 14 and 15 respectively. On the contrary, the formation water (FW) solution represent the worst-case scenario in altering the surface charge of the ILS core samples as indicated in Figure 14.
- These altered surface charges at both rock/fluid and fluid/fluid interfaces cause the brine/rock interface and the brine/oil interface to have the same sign (e.g., in the case of 100% $MgCl_2$ SW solution), resulting in a stable water film as shown in Figure 26 (i.e., zeta potential measurements). In contrast, when the brine/rock interface and the brine/oil interface have different zeta potential signs (e.g., in the case of formation water or FW solution), the water film will collapse (i.e., see Figure 26) [30,31].
- Furthermore, to generate the surfactant aqueous solutions (SAS), four types of surfactants (i.e., anionic and cationic) were mixed with selected smart water solutions candidates at different surfactant concentrations.
- Foamability and foam stability tests using the R5 parameter method were conducted to assess the best SAS formulations that ensure stable foam generation and the propagation inside the porous media during the dynamic mode (i.e., core flooding).
- The highest foam stability was attained at 90% when CTAB + AOS (i.e., 1000 ppm) was mixed with $MgCl_2$ (i.e., 3500 ppm) and nitrogen.
- A significant concern when using foam for mobility control is its stability in the presence of oil. In the presence of crude oil, foam generation and stability were negatively affected as expected. Figure 32 show that in the presence of oil, all SAS solutions reveal lesser foam stability compared with those attained by Figure 31 (i.e., the R5 stability percentage decreases approximately 10%) [42].
- Based on the core flooding tests, the foaming and foam stability of $MgCl_2$ + CTAB + AOS with nitrogen in the presence of crude oil (Type A) showed excellent ultimate oil recovery and improved the displacement efficiency (i.e., 92% cumulative OIIC).
- The modes of injection, including slugs of SAS followed by gas followed by a slug of SAS flowed by gas, shows that the SAG (SAS alternating gas) mode appears to have better performance than other injection sequence scenarios in terms of oil recovery i.e., 42% incremental OIIC (see Figure 34), which represents an optimistic scenario (i.e., in the case of 100% $MgCl_2$ and CTAB at desired concentration of 1000 ppm).
- It should be noted that even the pessimistic scenario with 20% incremental recovery of SWAF process i.e., in the case of 25% $MgCl_2$ + 75% NaCl and CTAB at desired surfactant concentration (21%, as shown in Figure 34) is still higher than the one

obtained with the conventional EOR (i.e., average 17%), which is reported in the literature [96].

- The optimum SWAF injection scenario (i.e., 100% MgCl$_2$ and CTAB at 1000 ppm) is optimized by studying the effect of the slug size of the SWAF injection scenarios. It is observed that changing the slug size of the SWAF injection scenario from 5 PV to 2 PV)leads to more oil recovery. Additionally, reducing the slug size from 5 PV to 2 PV reduces the fluid circulation costs, thus lowering the CO$_2$ footprint

- In summary, it is expected that the novel hybrid SWAF process under optimum controlled conditions can make the proposed new hybrid EOR method economically and environmentally attractive.

Abbreviations

The following symbols are used in this manuscript:
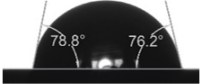
AST	Aqueous Solution Test
AOS	Alpha Olefin Sulfonate
CapEx	Capital Expenditures
CAT	Contact Angle Test
CF	Core-Flooding Test
COBR	Crude Oil Brine Rock
CT	Compatibility Test
CTAB	Cetyltrimethylammonium Bromide
DLVO	Derjaguin, Landau, Verwey, and Overbeek
EDL	Electrical Double Layer
EOR	Enhanced Oil Recovery
FST	Foam Stability Test
FT	Foamability Test
FW	Formation Water
IFT	Interfacial Tension
ILS	Indiana Limestone
LSW	Low Salinity Water
OIIC	Oil Initial In Core
OIIP	Oil initial In place
OpEx	Operational Expenditures
PDI	Potential Determining Ion
PV	Pore Volume

	SAG	SAS Alternating GAS
	SAS	Surfactant Aqueous Solution
	SCM	Surface Complexation Modeling
	SW	Smart Water
	SWAF	Smart Water-Assisted Foam
	TAN	Total Acid Number
	TBN	Total Base Number
	UCS	Unconfined Compressive Strength
	US	United States
	VdW	Van der Waals
	XRD	X-Ray Diffraction
	ZP	Zeta Potential
	ZPC	Zero Point of Charge
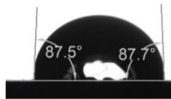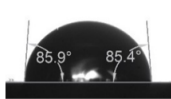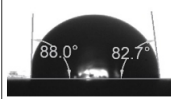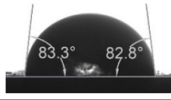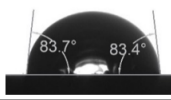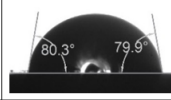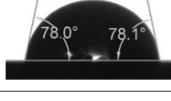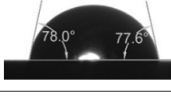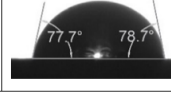
Appendix A. Contact Angle Measurements

	Repetition 1	Repetition 2	Average contact angle
0-hour			84.7°
24-hours			84.7°
48-hours			84.7°
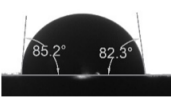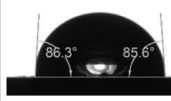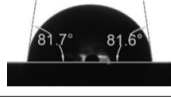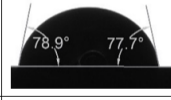
Figure A1. Dynamic Contact Angle Measurement Results for Sea-water (35,000 ppm).

	Repetition 1	Repetition 2	Repetition 3	Average contact angle
0 hour				86.9°
24 hours				77.3°
48 hours				72.5°
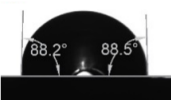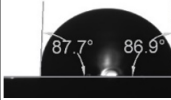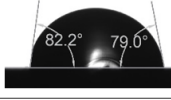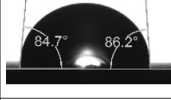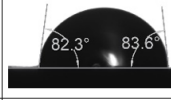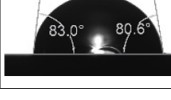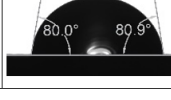
Figure A2. Dynamic Contact Angle Measurement Results for 20-times Diluted Sea-water (1750 ppm).

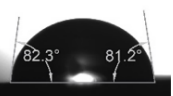|	Repetition 1	Repetition 2	Repetition 3	Average contact angle
0 hour	87.5° 87.7°	85.9° 85.4°	88.0° 82.7°	86.2°
24 hours	83.3° 82.8°	83.7° 83.4°	80.3° 79.9°	82.2°
48 hours	78.0° 78.1°	78.0° 77.6°	77.7° 78.7°	78.0°

Figure A3. Dynamic Contact Angle Measurement Results for 75% Na_2SO_4 + 25% $CaCl_2$ (3500 ppm).
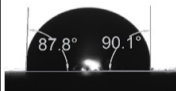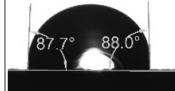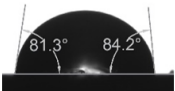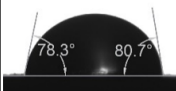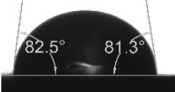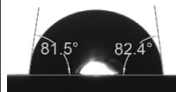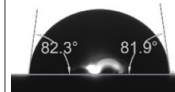
	Repetition 1	Repetition 2	Repetition 3	Average contact angle
0 hour	85.2° 82.3°	86.3° 85.6°	N/A	84.9°
24 hours	81.7° 81.6°	80.1° 81.7°	78.9° 77.7°	80.3°
48 hours	80.2° 82.7°	77.7° 75.8°	75.9° 76.9°	78.2°

Figure A4. Dynamic Contact Angle Measurement Results for $MgCl_2$ (3500 ppm).
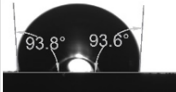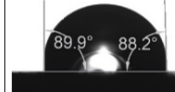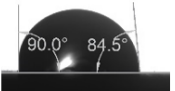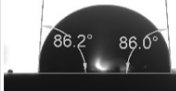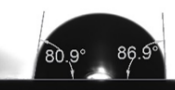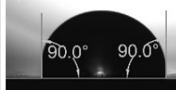
	Repetition 1	Repetition 2	Repetition 3	Average contact angle
0 hour	88.2° 88.5°	87.7° 86.9°	83.2° 84.2°	86.5°
24 hours	82.2° 79.0°	84.7° 86.2°	82.3° 83.6°	83.0°
48 hours	82.5° 73.7°	83.0° 80.6°	80.0° 80.9°	80.1°

Figure A5. Dynamic Contact Angle Measurement Results for 25% $MgCl_2$ + 75% NaCl (3500 ppm).
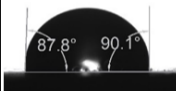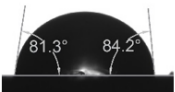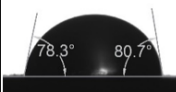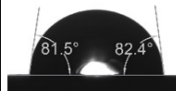
	Repetition 1	Repetition 2	Repetition 3	Average contact angle
0 hour	87.9° 87.7°	87.8° 90.1°	87.7° 88.0°	88.2°
24 hours	81.3° 84.2°	78.3° 80.7°	84.3° 83.5°	82.1°
48 hours	82.5° 81.3°	81.5° 82.4°	82.3° 81.9°	82.0°
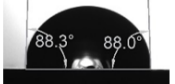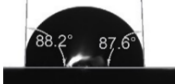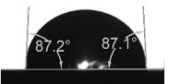
Figure A6. Dynamic Contact Angle Measurement Results for 50% $MgCl_2$ + 50% KCl (3500 ppm).

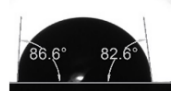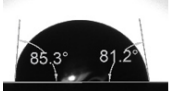|	Repetition 1	Repetition 2	Repetition 3	Average contact angle
0 hour	87.8° 86.9°	93.8° 93.6°	89.9° 88.2°	90.0°
24 hours	90.0° 84.5°	86.2° 86.0°	92.4° 92.0°	88.5°
48 hours	80.9° 86.9°	90.0° 90.0°	87.9° 87.8°	87.3°
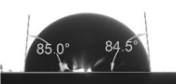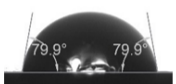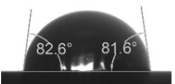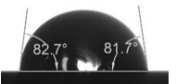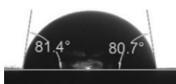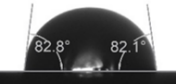
Figure A7. Dynamic Contact Angle Measurement Results for 25% $MgCl_2$ + 75% KCl (3500 ppm).

	Repetition 1	Repetition 2	Repetition 3	Average contact angle
0 hour	87.9° 87.7°	87.8° 90.1°	87.7° 88.0°	88.2°
24 hours	81.3° 84.2°	78.3° 80.7°	84.3° 83.5°	82.1°
48 hours	82.5° 81.3°	81.5° 82.4°	82.3° 81.9°	82.0°
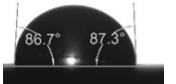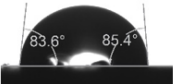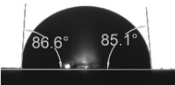
Figure A8. Dynamic Contact Angle Measurement Results for 50% $MgCl_2$ + 50% KCl (3500 ppm).

	Repetition 1	Repetition 2	Repetition 3	Average contact angle
0 hour	87.9° 87.6°	88.0° 87.5°	87.7° 86.9°	87.6°
24 hours	87.3° 87.8°	88.3° 88.0°	87.9° 86.0°	87.6°
48 hours	88.0° 87.2°	88.2° 87.6°	87.2° 87.1°	87.6°
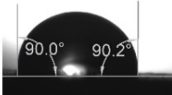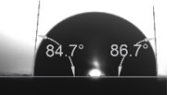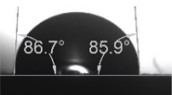
Figure A9. Dynamic Contact Angle Measurement Results for 75% $MgCl_2$ + 25% KCl (3500 ppm).

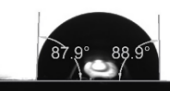|	Repetition 1	Repetition 2	Repetition 3	Average contact angle
0 hour	85.0° 84.5°	85.8° 85.1°	84.0° 83.4°	84.6°
24 hours	79.9° 79.9°	82.6° 81.6°	82.7° 81.7°	81.4°
48 hours	81.4° 80.7°	80.8° 80.3°	82.8° 82.1°	81.4°
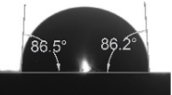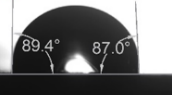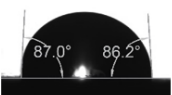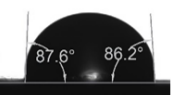
Figure A10. Dynamic Contact Angle Measurement Results for 50% $MgCl_2$ + 50% NaCl (3500 ppm).

	Repetition 1	Repetition 2	Repetition 3	Average contact angle
0 hour	86.7° 87.3°	83.6° 85.4°	88.0° 87.2°	86.4°
24 hours	86.5° 87.2°	86.6° 85.1°	86.2° 83.4°	85.8°
48 hours	86.3° 80.6°	83.5° 84.7°	84.2° 84.6°	84.0°
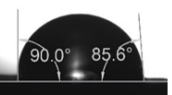
Figure A11. Dynamic Contact Angle Measurement Results for 75% $MgCl_2$ + 25% NaCl (3500 ppm).

	Repetition 1	Repetition 2	Repetition 3	Average contact angle
0 hour	90.0° 90.2°	89.7° 86.2°	87.7° 87.2°	88.5°
24 hours	89.9° 87.5°	84.7° 86.7°	86.7° 85.9°	86.9°
48 hours	87.1° 86.0°	84.5° 89.7°	87.0° 86.9°	86.9°
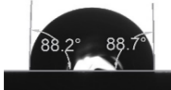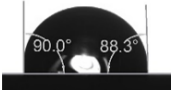
Figure A12. Dynamic Contact Angle Measurement Results for 25% $MgCl_2$ + 75% $CaCl_2$ (3500 ppm).

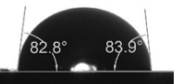|	Repetition 1	Repetition 2	Repetition 3	Average contact angle
0 hour	90.3° 88.1°	88.7° 87.8°	90.1° 89.9°	89.2°
24 hours	86.5° 86.2°	90.4° 85.6°	89.4° 87.0°	87.5°
48 hours	87.0° 86.2°	86.8° 87.6°	87.6° 86.2°	86.9°
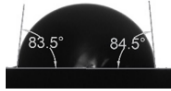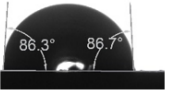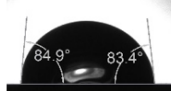
Figure A13. Dynamic Contact Angle Measurement Results for 50% $MgCl_2$ + 50% $CaCl_2$ (3500 ppm).

	Repetition 1	Repetition 2	Repetition 3	Average contact angle
0 hour	90.0° 85.6°	87.9° 90.0°	87.7° 90.0°	88.5°
24 hours	86.9° 87.2°	84.8° 85.2°	86.1° 85.6°	86.0°
48 hours	82.0° 83.6°	82.3° 81.2°	82.4° 83.9°	82.6°
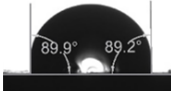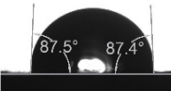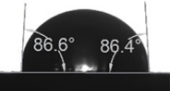
Figure A14. Dynamic Contact Angle Measurement Results for 75% $MgCl_2$ + 25% $CaCl_2$ (3500 ppm).

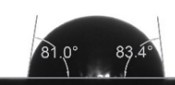|	Repetition 1	Repetition 2	Repetition 3	Average contact angle
0 hour	88.2° 88.7°	90.0° 88.3°	89.1° 88.1°	88.7°
24 hours	87.4° 85.0°	89.1° 88.8°	88.5° 90.3°	88.2°
48 hours	88.3° 88.1°	88.8° 87.1°	88.4° 87.7°	88.1°
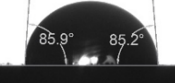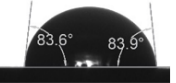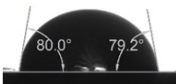
Figure A15. Dynamic Contact Angle Measurement Results for 25% $MgCl_2$ + 75% Na_2SO_4 (3500 ppm).

	Repetition 1	Repetition 2	Repetition 3	Average contact angle
0 hour	83.5° 84.5°	86.1° 86.1°	86.3° 86.7°	85.5°
24 hours	84.9° 83.4°	86.6° 82.6°	86.8° 86.8°	85.2°
48 hours	89.8° 83.9°	85.3° 81.2°	N/A	85.1°
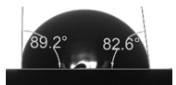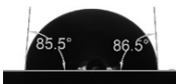
Figure A16. Dynamic Contact Angle Measurement Results for 50% $MgCl_2$ + 50% Na_2SO_4 (3500 ppm).

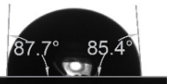|	Repetition 1	Repetition 2	Repetition 3	Average contact angle
0 hour	89.9° 89.2°	87.5° 87.4°	86.6° 86.4°	87.8°
24 hours	87.3° 84.8°	87.7° 90.0°	87.9° 88.9°	87.8°
48 hours	90.0° 86.9°	87.8° 86.5°	87.9° 87.4°	87.8°
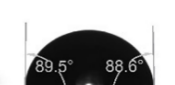
Figure A17. Dynamic Contact Angle Measurement Results for 75% $MgCl_2$ + 25% Na_2SO_4 (3500 ppm).

	Repetition 1	Repetition 2	Repetition 3	Average contact angle
0 hour	85.4° 85.0°	85.9° 85.2°	83.6° 83.9°	84.8°
24 hours	80.0° 79.2°	82.9° 78.6°	82.8° 83.9°	81.2°
48 hours	80.9° 79.6°	81.0° 83.4°	78.0° 84.0°	81.2°

Figure A18. Dynamic Contact Angle Measurement Results for 25% Na_2SO_4 + 75% $CaCl_2$ (3500 ppm).
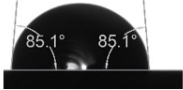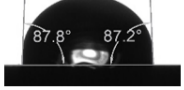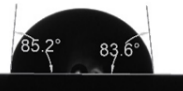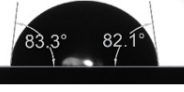
	Repetition 1	Repetition 2	Repetition 3	Average contact angle
0 hour	89.2° 82.6°	87.1° 85.6°	88.3° 87.8°	86.8°
24 hours	85.5° 86.5°	86.5° 88.3°	N/A	86.7°
48 hours	87.9° 86.0°	88.0° 85.0°	87.7° 85.4°	86.7°

Figure A19. Dynamic Contact Angle Measurement Results for 50% Na_2SO_4 + 50% $CaCl_2$ (3500 ppm).
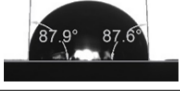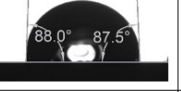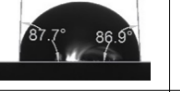
	Repetition 1	Repetition 2	Repetition 3	Average contact angle
0 hour	90.1° 90.1°	87.6° 90.0°	87.1° 87.5°	88.7°
24 hours	88.8° 85.3°	89.5° 88.6°	90.9° 86.5°	88.3°
48 hours	88.7° 87.4°	89.0° 88.5°	86.7° 88.2°	88.1°

Figure A20. Dynamic Contact Angle Measurement Results for 25% Na_2SO_4 + 75% KCl (3500 ppm).
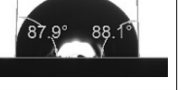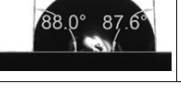
	Repetition 1	Repetition 2	Average contact angle
0 hour	85.1° 85.1°	87.8° 87.2°	86.3°
24 hours	85.2° 83.6°	82.9° 82.6°	83.4°
48 hours	83.3° 82.1°	83.7° 82.3°	82.9°
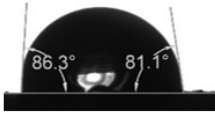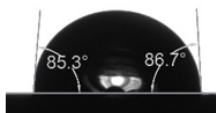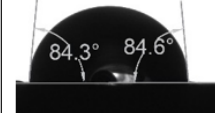
Figure A21. Dynamic Contact Angle Measurement Results for 50% Na_2SO_4 + 50% KCl (3500 ppm).

	Repetition 1	Repetition 2	Repetition 3	Average contact angle
0 hour	87.9° 87.6°	88.0° 87.5°	87.7° 86.9°	87.6°
24 hours	87.3° 87.8°	88.3° 88.0°	87.9° 86.0°	87.6°
48 hours	88.0° 87.2°	88.2° 87.6°	87.2° 87.1°	87.6°
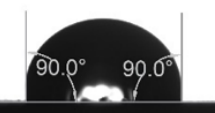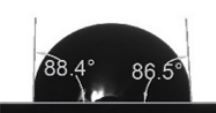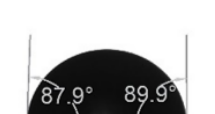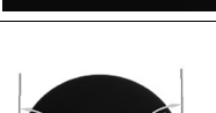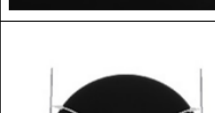
Figure A22. Dynamic Contact Angle Measurement Results for 75% Na_2SO_4 + 25% KCl (3500 ppm).

	Repetition 1	Repetition 2	Repetition 3	Average contact angle
0 hour	88.4° 87.9°	87.9° 88.1°	88.1° 86.7°	87.9°
24 hours	88.2° 88.0°	87.5° 88.5°	87.2° 86.2°	87.6°
48 hours	87.3° 87.6°	88.0° 87.6°	86.8° 87.3°	87.4°

Figure A23. Dynamic Contact Angle Measurement Results for 25% Na_2SO_4 + 75% NaCl (3500 ppm).

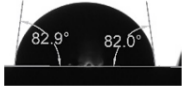|	Repetition 1	Repetition 2	Repetition 3	Average contact angle
0 hour	86.3° 81.1°	85.3° 86.7°	84.3° 84.6°	84.7°
24 hours	87.2° 80.6°	83.0° 84.0°	84.9° 84.2°	84.0°
48 hours	83.2° 82.7°	85.1° 84.7°	N/A	83.9°

Figure A24. Dynamic Contact Angle Measurement Results for 50% Na_2SO_4 + 50% NaCl (3500 ppm).

	Repetition 1	Repetition 2	Repetition 3	Average contact angle
0 hour	90.0° 90.0°	88.4° 86.5°	90.2° 88.4°	88.9°
24 hours	87.9° 89.9°	88.7° 87.8°	90.0° 87.8°	88.7°
48 hours	88.5° 87.0°	89.5° 88.8°	88.5° 88.7°	88.5°

Figure A25. Dynamic Contact Angle Measurement Results for 75% Na_2SO_4 + 25% NaCl (3500 ppm).

References

1. British Petroleum. *BP Statistical Review of World Energy*; BP: London, UK, 2020.
2. Global BP. *BP Energy Outlook*; Technical Report; 2018. Available online: https://www.bp.com (accessed on 18 January 2022).
3. Bai, G.; Xu, Y. Giant fields retain dominance in reserves growth. *Oil Gas J.* **2014**, *122*, 44–51.
4. Alvarado, V.; Manrique, E. Enhanced oil recovery: An update review. *Energies* **2010**, *3*, 1529–1575. [CrossRef]
5. Akbar, M.; Vissapragada, B.; Alghamdi, A.H.; Allen, D.; Herron, M.; Carnegie, A.; Dutta, D.; Olesen, J.R.; Chourasiya, R.; Logan, D. A snapshot of carbonate reservoir evaluation. *Oilfield Rev.* **2000**, *12*, 20–21.
6. Roehl, P.O.; Choquette, P.W. *Carbonate Petroleum Reservoirs*; Springer Science & Business Media: Berlin/Heidelberg, Germany,2012.
7. Kokal, S.; Al-Kaabi, A. Enhanced oil recovery: Challenges & opportunities. *World Pet. Counc. Off. Publ.* **2010**, *64*, 64–69.
8. Taber, J.; Martin, F.; Seright, R. EOR Screening Criteria Revisited-P1: Introduction to Screening and EOR Field Projects. Part 2: Applications and Impact of Oil Prices. *SPE Reserv. Eng.* **1997**, 189–220. [CrossRef]
9. Sheng, J.J. *Enhanced Oil Recovery Field Case Studies*; Gulf Professional Publishing; Elsevier: Amsterdam, The Netherlands, 2013. Available online: www.elsevier.com/permissions (accessed on 18 January 2022).

10. Moreno-Arciniegas, L.; Babadagli, T. Experimental analysis of optimal thermodynamic conditions for heavy-oil/bitumen recovery considering effective solvent retrieval. *SPE Reserv. Eval. Eng.* **2017**, *20*, 149–160. [CrossRef]

11. Hartono, A.; Hakiki, F.; Syihab, Z.; Ambia, F.; Yasutra, A.; Sutopo, S.; Efendi, M.; Sitompul, V.; Primasari, I.; Apriandi, R. *Revisiting EOR Projects in Indonesia through Integrated Study: EOR Screening, Predictive Model, and Optimisation*; OnePetro; The Society of Petroleum Engineers (SPE): Richardson, TX, USA, 2017.

12. Lake, L.W.; Johns, R.; Rossen, W.R.; Pope, G.A. *Fundamentals of Enhanced Oil Recovery*; The Society of Petroleum Engineers (SPE): Richardson, TX, USA, 2014.

13. Lee, J.; Nikolov, A.; Wasan, D. Stability of aqueous foams in the presence of oil: On the importance of dispersed vs solubilized oil. *Ind. Eng. Chem. Res.* **2013**, *52*, 66–72. [CrossRef]

14. Lee, S.; Kam, S. *Enhanced Oil Recovery Field Case Studies: Chapter 2. Enhanced Oil Recovery by Using CO_2 Foams: Fundamentals and Field Applications*; Elsevier Inc.: Amsterdam, The Netherlands, 2013.

15. Cuiec, L. Rock/crude-oil interactions and wettability: An attempt to understand their interrelation. In *SPE Annual Technical Conference and Exhibition*; OnePetro; The Society of Petroleum Engineers (SPE): Richardson, TX, USA, 1984.

16. Al-Shalabi, E.W. A New Insight into Modeling of Polymer Flooding in Carbonate Reservoirs. In *SPE Latin American and Caribbean Petroleum Engineering Conference*; OnePetro; The Society of Petroleum Engineers (SPE): Richardson, TX, USA, 2020.

17. Xu, Z.X.; Li, S.Y.; Li, B.F.; Chen, D.Q.; Liu, Z.Y.; Li, Z.M. A review of development methods and EOR technologies for carbonate reservoirs. *Pet. Sci.* **2020**, *17*, 990–1013. [CrossRef]

18. Lake, L.W. *Enhanced Oil Recovery*; Book, OCLC Number: 18134781; Prentice Hall: Englewood Cliffs, NJ, USA, 1989.

19. Rossen, W.R. Foams in enhanced oil recovery. *Foam. Theory Meas. Appl.* **1996**, *57*, 413–464.

20. Hassan, A.; Ayoub, M.; Eissa, M.; Bruining, H.; Al-Mansour, A.; Al-Quraishi, A. A New Hybrid Improved and Enhanced Oil Recovery IOR/EOR Process Using Smart Water Assisted Foam SWAF Flooding in Carbonate Rocks; A Laboratory Study Approach. In *International Petroleum Technology Conference*; OnePetro; The Society of Petroleum Engineers (SPE): Richardson, TX, USA, 2021.

21. Yuncong, G.; Mifu, Z.; Jianbo, W.; Chang, Z. Performance and gas breakthrough during CO_2 immiscible flooding in ultra-low permeability reservoirs. *Pet. Explor. Dev.* **2014**, *41*, 88–95.

22. Masalmeh, S.K.; Wei, L.; Blom, C. Mobility control for gas injection in heterogeneous carbonate reservoirs: Comparison of foams versus polymers. In *SPE Middle East Oil and Gas Show and Conference*; OnePetro; The Society of Petroleum Engineers (SPE): Richardson, TX, USA, 2011.

23. Dullien, F.; Chatzis, I.; Kantzas, A. Laboratory studies of macroscopic and microscopic mechanisms of immiscible gas drive-gravity drainage recovery. In Proceeding of the 3rd International Symposium on Enhanced Oil Recovery and III Simposio International Sobre Recuperacion Mejorada de Crudo, Maracaibo, Venezuela, February 1989; Volume 1, pp. 424–437.

24. Tunio, S.Q.; Chandio, T.A.; Memon, M.K. Comparative study of FAWAG and SWAG as an effective EOR technique for a Malaysian field. *Res. J. Appl. Sci. Eng. Technol.* **2012**, *4*, 645–648.

25. Aarra, M.; Skauge, A.; Martinsen, H. FAWAG: A Breakthrough for EOR in the North Sea. In *SPE Annual Technical Conference and Exhibition*; OnePetro; The Society of Petroleum Engineers (SPE): Richardson, TX, USA, 2002.

26. Blaker, T.; Aarra, M.G.; Skauge, A.; Rasmussen, L.; Celius, H.K.; Martinsen, H.A.; Vassenden, F. Foam for gas mobility control in the Snorre field: The FAWAG project. *SPE Reserv. Eval. Eng.* **2002**, *5*, 317–323. [CrossRef]

27. Simjoo, M.; Rezaei, T.; Andrianov, A.; Zitha, P. Foam stability in the presence of oil: Effect of surfactant concentration and oil type. *Colloids Surfaces A Physicochem. Eng. Asp.* **2013**, *438*, 148–158. [CrossRef]

28. Farajzadeh, R.; Andrianov, A.; Krastev, R.; Hirasaki, G.; Rossen, W.R. Foam–oil interaction in porous media: Implications for foam assisted enhanced oil recovery. *Adv. Colloid Interface Sci.* **2012**, *183*, 1–13. [CrossRef]

29. Hassan, A.; Ayoub, M.; Eissa, M.; Bruining, H.; Al-Mansour, A.; Al-Guraishi, A. A Novel Hybrid Enhanced Oil Recovery Method by Smart Water-Injection and Foam-Flooding in Carbonate Reservoirs. In *SPE/IATMI Asia Pacific Oil & Gas Conference and Exhibition*; OnePetro; The Society of Petroleum Engineers (SPE): Richardson, TX, USA, 2019.

30. Hassan, A.M.; Ayoub, M.; Eissa, M.; Bruining, H.; Zitha, P. Study of surface complexation modeling on a novel hybrid enhanced oil recovery (EOR) method; smart-water assisted foam-flooding. *J. Pet. Sci. Eng.* **2020**, *195*, 107563. [CrossRef]

31. Hassan, A.; Ayoub, M.; Eissa, M.; Bruining, H.; Al-Mansour, A.; Al-Guraishi, A. A Study of Combined Low Salinity Foam Injection Using DLVO Theory and Surface Complexation Modeling. In *Offshore Technology Conference Asia. Offshore Technology Conference*; OnePetro; The Society of Petroleum Engineers (SPE): Richardson, TX, USA, 2020.

32. Hassan, A.M.; Ayoub, M.; Eissa, M.; Musa, T.; Bruining, H.; Farajzadeh, R. Exergy return on exergy investment analysis of natural-polymer (Guar-Arabic gum) enhanced oil recovery process. *Energy* **2019**, *181*, 162–172. [CrossRef]

33. Bera, A.; Belhaj, H. Application of nanotechnology by means of nanoparticles and nanodispersions in oil recovery-A comprehensive review. *J. Nat. Gas Sci. Eng.* **2016**, *34*, 1284–1309. [CrossRef]

34. Nazari Moghaddam, R.; Bahramian, A.; Fakhroueian, Z.; Karimi, A.; Arya, S. Comparative study of using nanoparticles for enhanced oil recovery: wettability alteration of carbonate rocks. *Energy Fuels* **2015**, *29*, 2111–2119. [CrossRef]

35. Manan, M.; Farad, S.; Piroozian, A.; Esmail, M. Effects of nanoparticle types on carbon dioxide foam flooding in enhanced oil recovery. *Pet. Sci. Technol.* **2015**, *33*, 1286–1294. [CrossRef]

36. Olayiwola, S.O.; Dejam, M. A comprehensive review on interaction of nanoparticles with low salinity water and surfactant for enhanced oil recovery in sandstone and carbonate reservoirs. *Fuel* **2019**, *241*, 1045–1057. [CrossRef]

37. Sagala, F.; Montoya, T.; Hethnawi, A.; Vitale, G.; Nassar, N.N. Nanopyroxene-based nanofluids for enhanced oil recovery in sandstone cores at reservoir temperature. *Energy Fuels* **2019**, *33*, 877–890. [CrossRef]

38. Norrman, J.; Solberg, A.; Sjoblom, J.; Paso, K. Nanoparticles for waxy crudes: Effect of polymer coverage and the effect on wax crystallization. *Energy Fuels* **2016**, *30*, 5108–5114. [CrossRef]

39. Franco, C.A.; Nassar, N.N.; Ruiz, M.A.; Pereira-Almao, P.; Cortés, F.B. Nanoparticles for inhibition of asphaltenes damage: Adsorption study and displacement test on porous media. *Energy Fuels* **2013**, *27*, 2899–2907. [CrossRef]

40. Hou, B.; Jia, R.; Fu, M.; Wang, Y.; Jiang, C.; Yang, B.; Huang, Y. Wettability alteration of oil-wet carbonate surface induced by self-dispersing silica nanoparticles: Mechanism and monovalent metal ion's effect. *J. Mol. Liq.* **2019**, *294*, 111601. [CrossRef]

41. Jang, H.; Lee, W.; Lee, J. Nanoparticle dispersion with surface-modified silica nanoparticles and its effect on the wettability alteration of carbonate rocks. *Colloids Surfaces A Physicochem. Eng. Asp.* **2018**, *554*, 261–271. [CrossRef]

42. Hassan, A.M.; Ayoub, M.; Eissa, M.; Al-Shalabi, E.W.; Almansour, A.; Alquraishi, A. Foamability and Foam Stability Screening for Smart Water Assisted Foam Flooding: A New Hybrid EOR Method. In *International Petroleum Technology Conference*; OnePetro; The Society of Petroleum Engineers (SPE): Richardson, TX, USA, 2022.

43. Keller, S.J.; Becker, L.E. Subsurface stratigraphy and oil fields in the Salem Limestone and associated rocks in Indiana. In *Technical Report, Indiana Geological Survey*; Indiana Geological Survey, Department of Natural Resources: Indianapolis, IN, USA, 1980.

44. Buckley, E.R.; Buehler, H.A. *The Quarrying Industry of Missouri*; Volume 2; Tribune Printing Company, State Printers and Binders: California, CA, USA 1904.

45. Castro, P.; Huber, M. *Marine Biology Ed ke-5*; Mc Graw HillInternational: New York, NY, USA, 2005; pp. 119–125.

46. Manshad, A.K.; Nowrouzi, I.; Mohammadi, A.H. Effects of water soluble ions on wettability alteration and contact angle in smart and carbonated smart water injection process in oil reservoirs. *J. Mol. Liq.* **2017**, *244*, 440–452. [CrossRef]

47. Purswani, P.; Tawfik, M.S.; Karpyn, Z.T. Factors and mechanisms governing wettability alteration by chemically tuned water-flooding: A review. *Energy Fuels* **2017**, *31*, 7734–7745. [CrossRef]

48. Abdallah, W.; Buckley, J.S.; Carnegie, A.; Edwards, J.; Herold, B.; Fordham, E.; Graue, A.; Habashy, T.; Seleznev, N.; Signer, C.; et al. Fundamentals of wettability. *Technology* **1986**, *38*, 268.

49. Chilingar, G.V.; Yen, T. Some notes on wettability and relative permeabilities of carbonate reservoir rocks, II. *Energy Sources* **1983**, *7*, 67–75. [CrossRef]

50. Anderson, W.G. Wettability literature survey-part 1: Rock/oil/brine interactions and the effects of core handling on wettability. *J. Pet. Technol.* **1986**, *38*, 1125–1144. [CrossRef]

51. Donaldson, E.C.; Thomas, R.D.; Lorenz, P.B. Wettability determination and its effect on recovery efficiency. *Soc. Pet. Eng. J.* **1969**, *9*, 13–20. [CrossRef]

52. Donaldson, E.C.; Alam, W. *Wettability*; Elsevier: Amsterdam, The Netherlands, 2013.

53. Ding, H.; Rahman, S. Experimental and theoretical study of wettability alteration during low salinity water flooding-an state of the art review. *Colloids Surfaces A Physicochem. Eng. Asp.* **2017**, *520*, 622–639. [CrossRef]

54. Zhang, P.; Austad, T. Waterflooding in Chalk–Relationship between Oil Recovery, New Wettability Index, Brine Composition and Cationic Wettability Modifier (SPE94209). In Proceedings of the 67th EAGE Conference & Exhibition. European Association of Geoscientists & Engineers, Madrid, Spain, 13–16 June 2005; OnePetro; The Society of Petroleum Engineers (SPE): Richardson, TX, USA, 2005

55. Purswani, P.; Karpyn, Z.T. Laboratory investigation of chemical mechanisms driving oil recovery from oil-wet carbonate rocks. *Fuel* **2019**, *235*, 406–415. [CrossRef]

56. Shabib-Asl, A.; Ayoub, M.; Elraies, K. Laboratory investigation into wettability alteration by different low salinity water compositions in sandstone rock. In *SPE/IATMI Asia Pacific Oil & Gas Conference and Exhibition*; OnePetro; The Society of Petroleum Engineers (SPE): Richardson, TX, USA, 2015.

57. Hirasaki, G. *Wettability: Fundamentals and Surface Forces*; OnePetro; The Society of Petroleum Engineers (SPE): Richardson, TX, USA, 1991; Volume 6, pp. 217–226.

58. Mahani, H.; Keya, A.L.; Berg, S.; Bartels, W.B.; Nasralla, R.; Rossen, W.R. Insights into the mechanism of wettability alteration by low-salinity flooding (LSF) in carbonates. *J. Energy Fuels* **2015**, *29*, 1352–1367. [CrossRef]

59. Zhang, D. *Surfactant-Enhanced Oil Recovery Process for a Fractured, Oil-Wet Carbonate Reservoir*; School Rice University: Santiago, Region Metropolitana, 2005.

60. Lunkenheimer, K.; Malysa, K. Simple and generally applicable method of determination and evaluation of foam properties. *J. Surfactants Deterg.* **2003**, *6*, 69–74. [CrossRef]

61. Małysa, K.; Miller, R.; Lunkenheimer, K. Relationship between foam stability and surface elasticity forces: fatty acid solutions. *Colloids Surfaces* **1991**, *53*, 47–62. [CrossRef]

62. Lunkenheimer, K.; Małysa, K.; Wienskol, G.; Barańska, M. Method and Procedure for Swift Characterization of Foamability and Foam Stability. Patent (EP1416261A3), 16 January 2008.

63. Chandrasekhar, S.; Sharma, H.; Mohanty, K.K. Wettability alteration with brine composition in high temperature carbonate rocks. In *SPE Annual Technical Conference and Exhibition*; OnePetro; The Society of Petroleum Engineers (SPE): Richardson, TX, USA, 2016.

64. Yousef, A.A.; Al-Saleh, S.; Al-Kaabi, A.U.; Al-Jawfi, M.S. Laboratory investigation of novel oil recovery method for carbonate reservoirs. In *Canadian Unconventional Resources and International Petroleum Conference*; OnePetro; The Society of Petroleum Engineers (SPE): Richardson, TX, USA, 2010.

65. Yousef, A.A.; Al-Saleh, S.H.; Al-Kaabi, A.; Al-Jawfi, M.S. Laboratory investigation of the impact of injection-water salinity and ionic content on oil recovery from carbonate reservoirs. *SPE Reserv. Eval. Eng.* **2011**, *14*, 578–593. [CrossRef]

66. Alameri, W.; Teklu, T.; Graves, R.; Kazemi, H.; AlSumaiti, A. Low-salinity water-alternate-surfactant in Low-permeability Carbonate Reservoirs. In *IOR 2015–18th European Symposium on Improved Oil Recovery*; European Association of Geoscientists & Engineers: **2015**, p. 445. [CrossRef]

67. Fathi, S.J.; Austad, T.; Strand, S. "Smart water" as a wettability modifier in chalk: The effect of salinity and ionic composition. *Energy Fuels* **2010**, *24*, 2514–2519. [CrossRef]

68. Fathi, S.J.; Austad, T.; Strand, S. Water-based enhanced oil recovery (EOR) by "smart water": Optimal ionic composition for EOR in carbonates. *Energy Fuels* **2011**, *25*, 5173–5179. [CrossRef]

69. Fathi, J. Water-Based Enhanced Oil Recovery (EOR) in Carbonate Reservoirs: Initial Wetting Condition and Wettability Alteration by Smart Water. Ph.D. Thesis, University of Stavanger, Stavanger, Norway, 2012.

70. Su, W.; Liu, Y.; Pi, J.; Chai, R.; Li, C.; Wang, Y. Effect of water salinity and rock components on wettability alteration during low-salinity water flooding in carbonate rocks. *Arab. J. Geosci.* **2018**, *11*, 260. [CrossRef]

71. Karimi, M.; Al-Maamari, R.S.; Ayatollahi, S.; Mehranbod, N. Mechanistic study of wettability alteration of oil-wet calcite: The effect of magnesium ions in the presence and absence of cationic surfactant. *Colloids Surfaces A Physicochem. Eng. Asp.* **2015**, *482*, 403–415. [CrossRef]

72. Karimi, M.; Al-Maamari, R.S.; Ayatollahi, S.; Mehranbod, N. Wettability alteration and oil recovery by spontaneous imbibition of low salinity brine into carbonates: Impact of Mg^{2+}, SO_4^{2-} and cationic surfactant. *J. Pet. Sci. Eng.* **2016**, *147*, 560–569. [CrossRef]

73. Gomari, K.R.; Hamouda, A.; Denoyel, R. Influence of sulfate ions on the interaction between fatty acids and calcite surface. *Colloids Surfaces A Physicochem. Eng. Asp.* **2006**, *287*, 29–35. [CrossRef]

74. Zhang, P.; Austad, T. Wettability and oil recovery from carbonates: Effects of temperature and potential determining ions. *Colloids Surfaces A Physicochem. Eng. Asp.* **2006**, *279*, 179–187. [CrossRef]

75. Zhang, P.; Tweheyo, M.T.; Austad, T. Wettability alteration and improved oil recovery by spontaneous imbibition of seawater into chalk: Impact of the potential determining ions Ca^{2+}, Mg^{2+}, and SO_4^{2-}. *Colloids Surfaces A Physicochem. Eng. Asp.* **2007**, *301*, 199–208. [CrossRef]

76. Rashid, S.; Mousapour, M.S.; Ayatollahi, S.; Vossoughi, M.; Beigy, A.H. Wettability alteration in carbonates during "Smart Waterflood": Underlying mechanisms and the effect of individual ions. *Colloids Surfaces A Physicochem. Eng. Asp.* **2015**, *487*, 142–153. [CrossRef]

77. Shehata, A.M.; Alotaibi, M.B.; Nasr-El-Din, H.A. Waterflooding in carbonate reservoirs: Does the salinity matter. *SPE Reserv. Eval. Eng.* **2014**, *17*, 304–313. [CrossRef]

78. Romanuka, J.; Hofman, J.; Ligthelm, D.J.; Suijkerbuijk, B.; Marcelis, F.; Oedai, S.; Brussee, N.; van der Linde, H.; Aksulu, H.; Austad, T. Low salinity EOR in carbonates. In *SPE Improved Oil Recovery Symposium*; OnePetro; The Society of Petroleum Engineers (SPE): Richardson, TX, USA, 2012.

79. Al-Attar, H.H.; Mahmoud, M.Y.; Zekri, A.Y.; Almehaideb, R.; Ghannam, M. Low-salinity flooding in a selected carbonate reservoir: Experimental approach. *J. Pet. Explor. Prod. Technol.* **2013**, *3*, 139–149. [CrossRef]

80. Austad, T.; Strand, S.; Høgnesen, E.; Zhang, P. Seawater as IOR fluid in fractured chalk. In *SPE International Symposium on Oilfield Chemistry*; OnePetro; The Society of Petroleum Engineers (SPE): Richardson, TX, USA, 2005.

81. Austad, T.; Strand, S.; Madland, M.V.; Puntervold, T.; Korsnes, R.I. Seawater in chalk: An EOR and compaction fluid. In *International Petroleum Technology Conference*; OnePetro; The Society of Petroleum Engineers (SPE): Richardson, TX, USA, 2007.

82. Austad, T. Water-based EOR in carbonates and sandstones: New chemical understanding of the EOR potential using "Smart Water". In *Enhanced Oil Recovery Field Case Studies*; Elsevier: Amsterdam, The Netherlands, 2013; pp. 301–335.

83. Yousef, A.A.; Al-Saleh, S.; Al-Jawfi, M.S. Improved/enhanced oil recovery from carbonate reservoirs by tuning injection water salinity and ionic content. In *SPE Improved Oil Recovery Symposium*; OnePetro; The Society of Petroleum Engineers (SPE): Richardson, TX, USA, 2012.

84. Sari, A.; Xie, Q.; Chen, Y.; Saeedi, A.; Pooryousefy, E. Drivers of low salinity effect in carbonate reservoirs. *Energy Fuels* **2017**, *31*, 8951–8958. [CrossRef]

85. Alroudhan, A.; Vinogradov, J.; Jackson, M. Zeta potential of intact natural limestone: Impact of potential-determining ions Ca, Mg and SO_4. *Colloids Surfaces A Physicochem. Eng. Asp.* **2016**, *493*, 83–98. [CrossRef]

86. Song, J.; Zeng, Y.; Wang, L.; Duan, X.; Puerto, M.; Chapman, W.G.; Biswal, S.L.; Hirasaki, G.J. Surface complexation modeling of calcite zeta potential measurements in brines with mixed potential determining ions (Ca^{2+}, CO_3^{2-}, Mg^{2+}, SO_4^{2-}) for characterizing carbonate wettability. *J. Colloid Interface Sci.* **2017**, *506*, 169–179. [CrossRef] [PubMed]

87. Awolayo, A.; Sarma, H.; AlSumaiti, A.M. A laboratory study of ionic effect of smart water for enhancing oil recovery in carbonate reservoirs. In *lSPE EOR Conference at Oil and Gas West Asia*; OnePetro; The Society of Petroleum Engineers (SPE): Richardson, TX, USA, 2014.

88. Alotaibi, M.B.; Nasr-El-Din, H.A.; Fletcher, J.J. Electrokinetics of limestone and dolomite rock particles. *SPE Reserv. Eval. Eng.* **2011**, *14*, 594–603. [CrossRef]

89. Alotaibi, M.B.; Cha, D.; Alsofi, A.M.; Yousef, A.A. Dynamic interactions of inorganic species at carbonate/brine interfaces: An electrokinetic study. *Colloids Surfaces A Physicochem. Eng. Asp.* **2018**, *550*, 222–235. [CrossRef]

90. Jackson, M.D.; Al-Mahrouqi, D.; Vinogradov, J. Zeta potential in oil-water-carbonate systems and its impact on oil recovery during controlled salinity water-flooding. *Sci. Rep.* **2016**, *6*, 37363. [CrossRef]

91. Suarez-Rivera, R.; Stenebråten, J.; Gadde, P.B.; Sharma, M.M. An Experimental Investigation of Fracture Propagation during Water Injection. In *International Symposium and Exhibition on Formation Damage Control*; OnePetro; The Society of Petroleum Engineers (SPE): Richardson, TX, USA, 2002.

92. Vikingstad, A.K.; Skauge, A.; Høiland, H.; Aarra, M. Foam–oil interactions analyzed by static foam tests. *Colloids Surfaces A Physicochem. Eng. Asp.* **2005**, *260*, 189–198. [CrossRef]

93. Vikingstad, A.K.; Aarra, M.G.; Skauge, A. Effect of surfactant structure on foam–oil interactions: Comparing fluorinated surfactant and alpha olefin sulfonate in static foam tests. *Colloids Surfaces A Physicochem. Eng. Asp.* **2006**, *279*, 105–112. [CrossRef]

94. Vikingstad, A.K.; Aarra, M.G. Comparing the static and dynamic foam properties of a fluorinated and an alpha olefin sulfonate surfactant. *J. Pet. Sci. Eng.* **2009**, *65*, 105–111. [CrossRef]

95. Shabib-Asl, A.; Ayoub, M.A.; Saaid, I.M.; Valentim, P.P.J. Experimental investigation into effects of crude oil acid and base number on wettability alteration by using different low salinity water in sandstone rock. *J. Jpn. Pet. Inst.* **2015**, *58*, 228–236. [CrossRef]

96. Babadagli, T. Development of mature oil fields—A review. *J. Pet. Sci. Eng.* **2007**, *57*, 221–246. [CrossRef]